# Growth factor–loaded sulfated microislands in granular hydrogels promote hMSCs migration and chondrogenic differentiation

Acta Biomaterialia 166 (2023) 69–84

Contents lists available at ScienceDirect

Acta Biomaterialia

journal homepage: www.elsevier.com/locate/actbio

Full length article

# Growth factor–loaded sulfated microislands in granular hydrogels promote hMSCs migration and chondrogenic differentiation

Anna Puiggalí-Jou[a], Maryam Asadikorayem[a], Katharina Maniura-Weber[b], Marcy Zenobi-Wong[a,*]

[a] Tissue Engineering + Biofabrication Laboratory, Department of Health Sciences & Technology, ETH Zürich, Otto-Stern-Weg 7, 8093 Zürich, Switzerland
[b] Laboratory for Biointerfaces, Empa, Swiss Federal Laboratories for Materials Science and Technology, 9014 St. Gallen, Switzerland

ARTICLE INFO

*Article history:*
Received 12 November 2022
Revised 30 March 2023
Accepted 31 March 2023
Available online 6 April 2023

*Keywords:*
Microgels
Cartilage
Regeneration
Growth factors
Cell migration
Hydrogels

ABSTRACT

Cell-based therapies for articular cartilage lesions are expensive and time-consuming; clearly, a one-step procedure to induce endogenous repair would have significant clinical benefits. Acellular heterogeneous granular hydrogels were explored for their injectability, cell-friendly cross-linking, and ability to promote migration, as well as to serve as a scaffold for depositing cartilage extracellular matrix. The hydrogels were prepared by mechanical sizing of bulk methacrylated hyaluronic acid (HAMA) and bulk HAMA incorporating sulfated HAMA (SHAMA). SHAMA's negative charges allowed for the retention of positively charged growth factors (GFs) (e.g., TGFB3 and PDGF-BB). Mixtures of HAMA and GF-loaded SHAMA microgels were annealed by enzymatic cross-linking, forming heterogeneous granular hydrogels with GF deposits. The addition of GF loaded sulfated microislands guided cell migration and enhanced chondrogenesis. Granular heterogeneous hydrogels showed increased matrix deposition and cartilage tissue maturation compared to bulk or homogeneous granular hydrogels. This advanced material provides an ideal 3D environment for guiding cell migration and differentiation into cartilage.

**Statement of significance**

Acellular materials which promote regeneration are of great interest for repair of cartilage defects, and they are more cost- and time-effective compared to current cell-based therapies. Here we develop an injectable, granular hydrogel system which promotes cell migration from the surrounding tissue, facilitating endogenous repair. The hydrogel architecture and chemistry were optimized to increase cell migration and extracellular matrix deposition. The present study provides quantitative data on the effect of microgel size and chemical modification on cell migration, growth factor retention and tissue maturation.



## 1. Introduction

Traumatic injuries to articular cartilage, left untreated, can predispose the affected joint to osteoarthritis (OA). OA places a significant burden on patients, whose functional impairment leads to a loss of independence, and on society, due to the large healthcare expenditure and loss of labour power. The number of standard cartilage-repair procedures (bone marrow stimulation or microfracture (MF), osteochondral transplantation, and autologous chondrocyte implantation) performed is still small, compared to total joint replacement [1]. Total joint arthroplasty, currently the only effective, long-term (15-25 years) treatment available, presents many drawbacks, such as postsurgical complications, infections, or limited lifetime of the implant. A treatment to prevent the progression of cartilage lesions to end-stage OA would be ideal but remains a significant challenge in orthopaedic medicine.

Tissue engineering (TE), cell-based therapies combined with scaffolds and biomolecules, is an ideal strategy for cartilage regeneration [2]. Although autologous chondrocyte- and mesenchymal stem cell (MSC)-based techniques have several advantages (e.g., faster regeneration and mechanical stability), cell-based therapies are time-consuming, costly, and have variable outcomes due to low cell-survival rates, exogenous infection, or poorly targeted cell delivery [3]. Furthermore, the EMA and FDA consider cell-based therapies to be combination products (both a medical device and a

* Corresponding author.
*E-mail address:* marcy.zenobi@hest.ethz.ch (M. Zenobi-Wong).

https://doi.org/10.1016/j.actbio.2023.03.045

biologic) that require an expensive and lengthy approval process; commercialisation is, therefore, complex, and only a few TE products have reached the market.

In recent years, homing endogenous cells to an injury site has been intensively explored for facilitating cartilage repair [4–12]. This strategy uses the host's regenerative capacity and relies on biofunctional scaffolds. An ideal scaffold should provide enough void space, structural support, and a suitable microenvironment to recruit endogenous cells and facilitate their chondrogenic differentiation. In this context, granular hydrogels are an exciting alternative to conventional bulk hydrogels [13]. They consist of micrometre-sized gels cross-linked through annealing or jammed through centrifugation [14–16]. Their modular nature [17–19], in combination with their injectability and tunable structural characteristics, presents limitless combinations to support tissue repair [15,20,21]. For example, there is compelling evidence that, thanks to their large void space, they can stimulate endogenous repair in tissues, including the myocardium [22], brain after stroke [23], and skin [24]. However, in cartilage tissue engineering, they have so far been chiefly used as cell-laden injectable microgels [25,26].

To guide cells to colonize acellular materials, growth factors (GFs) are essential, but their translation to clinical use has been limited [27]. One challenge is that GFs are poorly retained upon implantation, leading to low efficiency and undesired secondary effects [28]. Physiologically, GF interactions with extracellular matrix (ECM) components facilitate localised and spatially regulated signalling [29,30]. In the human body, they are retained mainly by heparin, the most negatively charged glycosaminoglycan in human ECM. Heparin's high binding affinity towards positively charged proteins (i.e., electrostatic interactions) has caused it to be used in TE for the delivery of GFs [31]. However, its fast degradation, impurity, anticoagulant properties, and desulfation present drawbacks [32,33]. In order to mimic the GF-binding affinity of heparin, we prepared sulfated hyaluronic acid and incorporated sulfated microislands into our granular hydrogel. Significantly, sulfated materials can instruct cells to undergo chondrogenesis. Recently, Chasan et al. compared differentially sulfated biomaterials and determined that sulfation can instruct directs cells to follow the chondral rather than the endochondral pathway [34]. Furthermore, much literature highlights the beneficial effects of sulfated polymers in chondrogenesis [35–37], but it has not been yet explored how their localization at the microscale affects cell behaviour.

Taking advantage of granular hydrogels' high modularity, we generated hot spots of growth factors (GFs) using sulfated microislands. Similar approaches have been explored for skin regeneration [31] or for osteoarthritis [38]; both showed better GF retention and subsequently enhanced MSC recruitment compared to approaches without controlled release of GFs. Interestingly, as shown by L. Pruett et al., cell migration was greater when granular gels were 10% heparin-containing particles, compared to 100% heparin-containing particles with the same total amount of GFs. This result confirmed that heterogeneity, and not simply heparin content, was responsible for the observed increase in *in vitro* cell migration [31].

PDGF-BB has been extensively used to recruit human MSCs, being more specific and potent than its dimer isoforms (e.g. PDGF-AA and PDGF-AB), IL-8 and SDF-1 [39–43]. It has also been shown that a combination of GFs can be beneficial in recruiting cells [44]. Liebesny et al. showed that PDGF-BB or TGF- $\beta$1 alone could not induce MSC migration, but their combination could [45]. In this study, we hypothesized that the combination of PDGF-BB and TGF-$\beta$3 would effectively promote cell migration and subsequent chondrodifferentation.

The goal of this study was to design a cell-free granular hydrogel material which promoted the recruitment of both MSCs from the subchondral bone and chondrocytes from the surrounding cartilage (Fig. 1). To achieve maximal repair, the void space, pore interconnectivity, and GF localization were studied to promote cartilage self-repair and overcome the significant limitations of MF (i.e., high failure rate and formation of fibrocartilage). Such a procedure could result in shorter operation times and lower overall costs compared to cell-based approaches like autologous chondrocyte implantation.

## 2. Materials and methods

### 2.1. Materials

Hyaluronic acid (HA) (intrinsic viscosity: 1.92 $m^3$/kg) was purchased from HTL Biotechnology. Gentamycin, Dulbecco's modified eagle medium (DMEM 31966) and fetal bovine serum (FBS) were obtained from Gibco. ITS+ Premix Universal Culture Supplement was purchased from Corning and fibroblast growth factor-2 (FGF-2) and transforming growth factor-$\beta$3 (TGF-$\beta$3) from PreproTech. Tetrabutylammonium hydroxide solution (TeBA-OH) (40%) was obtained from Fluka; all other reagents were from Merck. Fibrogammin (FXIII) was acquired from CSL Behring and thrombin (Thr) from Tissucol, Baxter.

### 2.2. Methods

#### 2.2.1. Hyaluronic acid methacrylate (HAMA) synthesis

Hyaluronic acid methacrylate (HAMA) was synthesised as described previously in the literature [46,47]. Briefly, 1% high molecular weight HA (1.2 MDa) was dissolved in ultrapure water overnight. The next day, the solution was placed in an ice bath and the pH was adjusted to 8.0 with NaOH. A 20-fold molar excess (per disaccharide unit) of methacrylic anhydride was added under vigorous stirring. During the first 3 h, the pH was maintained at 8.0 by adding 5 M NaOH, after which the reaction was allowed to proceed for 24 h at 4 °C. After 24 h, HAMA was precipitated by dripping the solution into an excess of ice-cold ethanol. The precipitate was then collected by vacuum filtration. After redissolving the precipitated HAMA in 0.5 M NaCl, the resulting solution was dialysed for 3 days against ultrapure water (Spectra/Por 5, MWCO 12–14 kDa). The water was changed two times every 24 h. The product was freeze-dried and stored at −20 °C before use. NMR spectroscopy ($D_2O$, 500 MHz) revealed successful methacrylation of the hyaluronan. The degree of substitution (DS) was calculated by the ratio of the integrals of the vinyl protons at 5.6 ppm and 6.1 ppm to the protons from the methyl groups of both HA and the methacryloyl residues at 1.9 ppm. The calculated DS for the batches used in this work ranged from 25–34.6%. Chemical synthesis scheme can be found in **Scheme S1**.

#### 2.2.2. Synthesis of sulfated hyaluronic acid methacrylate (SHAMA)

Sulfation of HAMA was carried out in a two-step procedure. In the first step, water-soluble HAMA becomes hydrophobic via substitution of the $Na^+$ ion with tetrabutylammonium hyaluronate ($TeBA^+$) to allow polymer solubility in dimethylformamide (DMF); and in the second step, sulfation is performed using sulfur trioxide pyridine complex ($SO_3$-Py) solution in DMF. Chemical synthesis scheme can be found in **Scheme S1**.

*2.2.2.1. Preparation of Tetrabutylammonium hyaluronate (TeBA-HAMA).* HAMA (1.17 g, 2.5 mmol) was dissolved in 100 mL of Milli-Q water to obtain 1.17% w/v polymer solution. 25 mL of 0.6 M HCl was gradually added to the solution and the solution was stirred for 6 h in an ice bath to complete the acidification of the HAMA. The solution was precipitated in cold ethanol, centrifuged, washed again with ethanol and dried under vacuum. The resultant hyaluronic acid was dissolved in 150 mL of Milli-Q water, and the

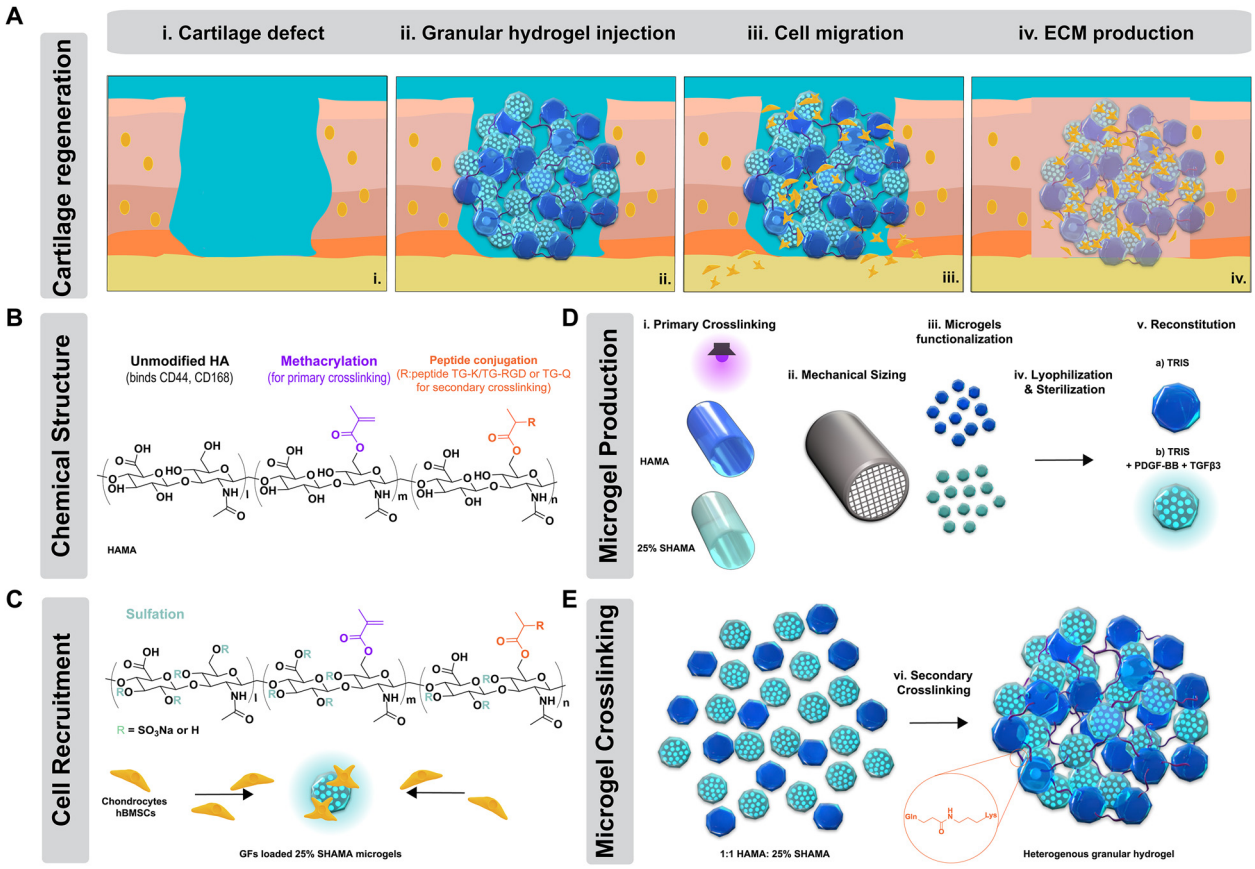


**Fig. 1.** Illustration of granular hydrogels for cell recruitment containing SHAMA microislands. A) A cartilage lesion can be filled with the injectable granular hydrogel and cross-linked *in situ*; after a few days, cells start migrating following the gradient generated by the GF-loaded 25% SHAMA microislands and start producing ECM. B) Chemical structure: macromers were designed from hyaluronic acid (to bind to specific cell receptors), modified with methacrylates for photocross-linking and with transglutaminase-sensitive peptides containing the RGD sequence, to permit secondary enzymatic annealing and cell spreading. C) Cell recruitment: 25 % SHAMA microislands were generated with the same modified HA but adding a third modification, sulfation. Sulfation allows for the retention of positively charged growth factors (PDGF-BB and TGF$\beta$3), forming microislands – microgels that can direct cells. D) Microgel production: bulk gels were produced by photopolymerising methacrylated hyaluronic acid, then mechanically fragmenting to obtain microgels; lyophilised, sterilised, and finally reconstituted in buffer with/without GFs (blue = HAMA, green = 25% SHAMA). E) Microgel cross-linking: preparation of SHAMA granular hydrogels by blending 25% SHAMA and HAMA microgels at a 1:1 ratio and annealing them by adding FXIII and Thr for 30 min at 37°C.

pH was carefully adjusted to 8 using 40% TeBA-OH solution. The solution was immediately frozen and then lyophilised.

*2.2.2.2. Preparation of sulfated HAMA (SHAMA).* Completely dried TeBA-HAMA (0.585 g) was dissolved in 100 mL anhydrous DMF at room temperature under nitrogen. $SO_3$-Py (2.75 g) was dissolved in 15 mL of DMF and added to the solution (Polymer/$SO_3$ 1:20). The solution was stirred for 3 h at room temperature under nitrogen. The reaction was quenched by adding 15 mL of cold water, after which the solution pH was adjusted to 8-9 by adding 1 M NaOH to obtain sodium salt of sulfated hyaluronic acid. The solution was precipitated in cold ethanol, centrifuged, washed again with ethanol and dried under vacuum. The resulting white powder was dissolved in Milli-Q-water, dialysed with Spectra/Pro membranes (MWCO 3500) against distilled water for 3 days, and then lyophilised resulting in a white foam. Fourier-transform infrared spectroscopy (FTIR) was performed to detect sulfate bands.

*2.2.3. HAMA peptide modification*

HAMA was functionalized with the following peptides: TG-Q (NQEQVSPL-ERCG), TG-K (TG/Lys: FKGG-ERCG), and TG-K/RGD (FKGG-ERCGG-RGD). The peptides containing a cysteine amino acid were conjugated to the HAMA backbone with a Michael addition reaction between the methacrylate groups and the thiol groups of each peptide [48,49]. HAMA (240 mg) was dissolved in 100 mL of 300 mM triethanolamine-buffered saline (pH 8) and reacted at 37°C overnight in the presence of 93.29 mg TG-Q or 58.21 mg TG-K or TG-K-RGD, followed by dialysis and lyophilization. This coupling ratio was designed to consume no more than 20% of available methacrylate groups on the HAMA.

*2.2.4. Bulk hydrogels preparation*

The different compositions were prepared as follows: HAMA gels were prepared with a 2% HAMA in PBS containing 0.05% lithium-phenyl-2,4,6,-trimethylbenzoylphosphinat (LAP). 25% SHAMA gels were prepared by 0.5% SHAMA and 1.5% HAMA in PBS containing 0.05% LAP. 50% SHAMA gels were prepared by 1% SHAMA and 1% HAMA in PBS containing 0.05% LAP. The solutions were irradiated by UV.VIS (405 nm) for 5 min.

*2.2.5. Granular hydrogel preparation*

Bulk hydrogels were cross-linked in transparent BD syringes. After cross-linking, the bulk gel was transferred into a 10 mL homemade extruder connected to a metal sieve with average aperture diameters of 20, 150 µm. Bulk gels were manually sieved three consecutive times, transferred into 2 mL Eppendorf and lyophilized. Lyophilized HAMA and SHAMA microgels, were split in equal parts, resuspended in triethanolamine-buffered saline (pH 8) and each part reacted at 37°C overnight in the presence of TG-Q or TG-K or TG-K/RGD, followed by 8 cleaning repetitions, centrifuged (18000 rpm, 10 min) with dH2O, and lyophilized. Finally, a solution of 6% w/v of microgels in TBG (50 mM TRIS, 200 mM D-glucose,

pH 7.6) + 100 mM CaCl2 was produced. To prepare 100 µL of homogenous granular hydrogel, 41.75 µL of microgels substituted with TG-Q were mixed with 41.75 µL of microgels substituted with TG-K or TG-K/RGD, 2.5 µL of thrombin (500 U/mL), 5 µL of FXIII (200U/mL), and 10 µL of buffer or cells. To prepare 100 µL of heterogeneous granular hydrogel, 20.9 µL of HAMA microgels substituted with TG-Q were mixed with 20.9 µL of HAMA microgels substituted with TG-K or TG-K/RGD, 20.9 µL of SHAMA microgels substituted with TG-Q, 20.9 µL of SHAMA microgels substituted with TG-K/RGD, 2.5 µL of thrombin (500 U/mL), 5 µL of FXIII (200U/mL), and 10 µL of buffer or cells. Therefore, presenting a ratio of 1:1 between HAMA and SHAMA microgels. The solutions were cast on PDMS molds and incubated at 37 °C for 30 min in a humid atmosphere.

*2.2.6. Size distribution*

HAMA bulk hydrogels were made by preparing 2% HAMA, 0.05% LAP, and 0.06 mg/mL fluorescein O-methacrylate in PBS. Bulk hydrogels were cross-linked in transparent BD syringes by UV-VIS (405 nm) irradiation for 5 min. After cross-linking, the bulk gel was transferred into a 10 mL homemade extruder connected to a metal sieve with average aperture diameters of 20, 150 µm. Bulk gels were manually sieved three consecutive times. Microgel size was determined by dispersing the microgels into glass slides and imaging with a fluorescent microscope (SP8, Leica). Microgel diameter was evaluated using imageJ software with the particle analysis tool.

*2.2.7. Scanning electron microscopy (SEM) and energy-dispersive X-ray (EDX)*

100 µL of HAMA, 25% SHAMA and 50% SHAMA solutions were cast in PDMS rings and UV cross-linked. The hydrogels were washed several times with $dH_2O$, snap-frozen in liquid nitrogen, fractured, and lyophilized. Samples were coated with a 10 nm carbon layer (CCU- 010 Carbon Coater Safematic). Then, samples were imaged with SEM (Zeiss Merlin) at an operating voltage of 3–5 kV.

*2.2.8. Enzymatic degradation*

Hydrogel precursors were cast into PDMS molds and enzymatically cross-linked or UV cross-linked for 30 min or 5 min, respectively. After cross-linking, gels were immersed in PBS for 1h and weighed. Afterwards, each gel was immersed into 1 mL of PBS solution containing 10 U/mL type II hyaluronidase from sheep testes. At regular intervals, the supernatants were gently removed and the samples weighed. Fresh hyaluronidase solution was added after each measurement to ensure constant enzymatic activity. The degradation rate was determined as the hydrogel mass at a given time divided by its initial mass.

*2.2.9. Swelling*

HAMA and SHAMA gel precursors were cast into five 4 × 1 mm-diameter PDMS molds, secondary cross-linked for 10 min, and transferred to 1.5 mL Eppendorf tubes containing 1 ml PBS. After 24 h, supernatants were removed and the samples weighed. The swelling ratio was calculated as the ratio of hydrogel mass at a given time point divided by its initial mass after 1 h of swelling.

*2.2.10. Mechanical testing*

Unconfined compression experiments were performed on a TA.XTplus texture Analyser (Anton Paar) equipped with a 500 g load cell. For each sample (4 mm in diameter and 1 mm in height), a pre-load was applied to the sample until it reached full contact with the plate and was then allowed to relax completely. Samples were compressed at a rate of 0.01 mm/s until they reached a 15% strain. The compressive modulus was extracted from the slope of the first 3% of the stress vs strain curve.

*2.2.11. Porosity calculation*

Bulk hydrogels were made by preparing 2% HAMA, 0.05% LAP, and 0.06 mg/mL Fluorescein methacrylate. Bulk hydrogel was sized and cross-linked as previously mentioned. Samples were imaged by confocal microscopy (SP8, Leica). Porosity and pore area were determined by converting the stacks into single images and using a threshold to select the void spaces. Cross-sectional areas occupied by void spaces were determined for each image and averaged for the whole stack.

*2.2.12. Percentage of microgel volume within the heterogenous granular hydrogels*

HAMA bulk hydrogels were made by preparing 2% HAMA, 0.05% LAP, and 0.06 mg/mL Fluorescein methacrylate in PBS. SHAMA bulk hydrogels were made by mixing 0.5% SHAMA, 1.5% HAMA and high-molecular-weight TRITC dextran (Mw ≃ 500 kDa) at a 1mg/mL concentration in PBS containing 0.05% LAP. Bulk hydrogel was sized, cross-linked and washed as previously mentioned. Samples were imaged by confocal microscopy (SP8, Leica). IMARIS software package was used to visualize the 3D reconstruction of the gel and calculate the volume fraction distribution of the two types of microgels within granular hydrogels.

*2.2.13. Rheology*

Hydrogel precursors were precisely loaded onto the centre of the bottom plate. The upper plate was lowered to a measuring gap size of 0.2 mm, ensuring proper loading of the space between the plates and gel precursors; the dynamic oscillating measurement was then started. Humidity in the thermal hood was controlled by placing a wet tissue inside to prevent drying of the sample. The evolution of storage modulus (G′) and loss modulus (G′′) were at a constant when equilibrium was reached, and measurement points were recorded every 20 s. Microgels were swollen in TBG (50 mM TRIS, 200 mM d-glucose, pH 7.6) + 100 mM $CaCl_2$, and cross-linking was performed by the addition of 12.5 U/mL FXIII and 10 U/mL Thr. The solution was immediately placed on the rheometer and the test started about 2 min after the addition of the enzymes. The measurements were performed on an Anton Paar MCR 301 rheometer at 37 °C equipped with a 20 mm parallel-plate geometry and a Peltier element equipped with a thermal hood (H-PTD 200, Anton Paar).

*2.2.14. Fluorescence recovery after photobleaching*

Stock solutions of FITC-dextran of 10 and 500 kDa were prepared at a concentration of 10 mg/mL in Tris buffer. Discs (12 µL) of the selected HAMA, 25% SHAMA and 50% SHAMA were formed in the presence of differently-sized FITC-dextran solutions at a final concentration of 1 mg/mL. Hydrogels were then equilibrated overnight at 37°C in a solution containing the same concentration of the corresponding FITC-dextran. FITC-dextran-loaded hydrogels were transferred to imaging chambers (µ-Slide 18-well glass bottom, Ibidi), and recovery curves were taken with a Leica TCS SP8 confocal microscope using the FRAP booster option with 20 × magnification objective and argon laser at 488 nm. A bleach spot of 20 µm diameter was selected for all measurements. The area was monitored by 15 pre-bleach image scans (500 ms interval) at a laser power of 1% and bleached by 3 image scans (83 ms interval) at 100% laser power. The fluorescent recovery was detected by 240 post-bleach image scans (500 ms interval), again at a low power of 1%. For the quantitative analysis, the Leica processing software was used, allowing to obtain the mobile fraction, T-half (half maximal recovery time); and the diffusion coefficient D was calculated by D = w2/T-half, where w is the radius of the bleached spot (20 µm).

*2.2.15. ELISA for quantification of PDGF-BB and TGFβ-3 release*

Lyophilized microgels were swollen overnight in TBG buffer containing 1.66 µg/mL of TGFβ-3 (Peprotech) and 8.3 µg/mL of PDGF-BB to reach a 6 w/v% of microgels in solution. Solutions were cast on PDMS molds and gelled as previously explained. Granular hydrogels were incubated in PBS 1X containing 0.1% (w/v) bovine serum albumin (BSA) for up to 2 weeks. At given time points, the buffer was replaced completely and was stored at −20°C until used. PDGF-BB and TGFβ-3 release from hydrogels was quantified by PDGF-BB and TGFβ-3 ELISA kits (R&D Systems) according to manufacturer protocols.

*2.2.16. Human BMSC isolation and culture*

Human bone marrow-derived stromal cells (hBMSCs) were isolated, as described previously, from bone marrow aspirates of healthy donors obtained during orthopedic surgical procedures after informed consent and in accordance with the local ethical committee (EKSG 08/14). Cells were cultured at 37°C in a humidified atmosphere at 5% $CO_2$ in minimal essential medium (MEMα) (with nucleosides, Gibco), supplemented with fetal bovine serum (FBS, 10%, Gibco), penicillin (100 U/mL, Gibco), gentamicin (100 µg/mL, Gibco), and fibroblast growth factor 2 (FGF-2, 5 ng/mL, PeproTech). Cells were passaged until they reached 90% confluency.

*2.2.17. Spheroid formation*

The cells were trypsinized, counted and stained with CellTracker Deep Red (Invitrogen). Specifically, cells were incubated for 30 min in suspension at 37 °C with 20 µM working solution (cell medium w/o serum). Cells were centrifuged to wash away the extra dye and resuspended at a concentration of 75000 cells/mL in a maintenance medium with 0.2% methyl cellulose and without FGF-2. Droplets of 10 µL were placed in non-adhesive cell culture dishes and cultured O/N as hanging drops. After 24 h, cells were harvested in maintenance medium and washed once with maintenance medium. Spheroids were then encapsulated on HAMA hydrogels at a final concentration of 250 spheroids per mL. Hydrogels were prepared in a 48-well plate with a PDMS ring as mold. Gels were cultured for 4 days in 500 µL of maintenance medium with and without PDGF. PDGF was purchased as lyophilized powder form Sigma Aldrich and re-suspended in 50 µM/mL Tris pH 7.6 supplemented with 0.1% bovine serum albumin. Afterwards, samples were washed with PBS and observed using confocal microscope (Leica SP-8). When evaluating collagen deposition Leica SP-8 multiphoton microscope equipped with a 25x water immersion objective was used. Excitation was performed at 900 nm (Mai Tai XF, Spectra-Physics) and second-harmonic generation collected from 440 to 550 nm.

*2.2.18. Time-lapse microscopy*

The µ-slide chemotaxis from ibidi was unpacked and put into a sterile Petri dish; a wet tissue was added around the slide to decrease evaporation. The cells were trypsinized, counted, and stained with CellTracker Red CMTPX (Invitrogen). Specifically, cells were incubated for 30 min in suspension at 37 °C with 20 µM working solution (cell medium w/o serum). Cells were centrifuged to wash away the extra dye and resuspended at concentration of 3 M cell/mL in HAMA, 20 µm sized-, or 150 µm sized-granular hydrogel. 6 µL of each sample was carefully pipetted onto the middle channel of the chambers. To the left reservoir we added 60 µL of DMEM containing 100 ng/mL of PDGF-BB and to the right only DMEM without any GF. After filling the ports, the lids were added, and the samples were left in the incubator for 2 h before starting the imaging. The sample was imaged on the Zeiss Apotome microscope with a 5x objective, and an image was taken every 15 min for 3 days. After that, videos were analysed with the TrackMate plugin from Fiji [50,51].

*2.2.19. Cell viability*

Viability was assessed by a Live/Dead staining. Samples were washed twice in PBS, stained for 20 min with 1 µM Calcein AM, 1 µM propidium iodide (PI) and 0.3 µM Hoechst, and washed again three times with PBS 1X for 10 min. Images were recorded on a Leica SP8 confocal equipped with a 10 × dry objective. 100 µm Z-stacks were acquired with 5 µm steps. Viability was determined after 21 days as the number of viable cells (Calcein AM) divided by the total number of cells (Calcein AM + PI).

*2.2.20. In vitro chondrogenesis*

HAMA and SHAMA granular hydrogels were cultured in chondrogenic medium containing DMEM, 10 µg/mL gentamycin, 1% ITS+, 50 µg/mL L-ascorbate-2-phosphate, 40 µg/mL L-proline, 10 ng/mL TGF-β3, and 0.1 µM dexamethasone. Medium was changed every 3–4 d. *In vitro* differentiation experiments were stopped after 21 days for mechanical and histological analysis.

*2.2.21. Histology and immunohistochemistry*

Samples were fixed in 4% paraformaldehyde for 2h and dehydrated in an ethanol sequence (20%, 40%, 60% and 70%, being 1h in each); finally, they were embedded in paraffin wax (Milestone LogosJ) and cut into 5 µm sections. All samples were progressively deparaffinized and rehydrated before staining. Brightfield images of stained sections were recorded on a 3DHistech Pannoramic 250-slide scanner and visualized with the case viewer 2.4 software. Safranin O staining was performed by staining in Weigert's Iron Hematoxylin for 5 min, differentiating in 1% acid-alcohol for 2 s, staining in 0.02% Fast Green solution for 1 min and rinsing with 1% acetic acid for 30 s. Finally, sections were stained in 1% Safranin O for 30 min. Hematoxylin and Eosin staining were performed by staining in Mayer's Hematoxylin for 8 min, rinsing under tap water for 10 min, and counterstaining with Eosin Y for 1 min.

Collagen I and II immunohistochemistry (IHC) staining were performed as previously described [52]. Antigen retrieval was first performed in hyaluronidase (1200 U/mL) at 37°C for 30 min. Sections were blocked with 5% bovine serum albumin (BSA) in PBS for 1 h. Primary antibody, mouse anti-collagen I (1:1500, ab138492, Abcam), and mouse anti-collagen II (1:20, II-II6B3-s, DSHB Hybridoma) were dissolved in 1% BSA in PBS, and sections were incubated overnight at 4°C. Sections were incubated with the secondary antibody, goat anti-mouse IgG-HRP for collagen II (1:1000, ab6789, Abcam), in 1% BSA in PBS for 1 h and developed with the DAB substrate kit (ab64238, Abcam) for 5 min. Sections were stained with Weigert's iron hematoxylin (Thermo Fisher Scientific) for 3 min, destained in 1% acid-alcohol, blued in 0.1% $Na_2CO_3$, dehydrated to xylene and mounted.

*2.2.22. Sample preparation for biochemical analysis*

The scaffolds were washed with $dH_2O$, frozen at -80°C and lyophilized overnight. Each sample was weighed before adding 500 µL of a 0.27 mg/mL solution of papain from Papaya Latex in a buffer containing 10 mM L-cysteine HCl, 100 mM sodium phosphate, and 10 mM EDTA in milliQ water, pH 6.3. The digestion was done at 60°C overnight with shaking (1000 rpm).

*2.2.23. DNA quantification (Picogreen)*

The amount of DNA was quantified using a Quant-iT PicoGreen dsDNA assay kit (Invitrogen) as per manufacturer's protocol. Briefly, the samples were pre-diluted in TE buffer. 50 µL of this dilution was transferred into a 96-well plate and 50 µL of Picogreen solution was added. The fluorescence was measured with a micro-plate reader (excitation 480 nm, emission 520 nm). The DNA content was calculated as ng DNA/mg gel; it was not normalized to day 0 because it was an acellular gel.

*2.2.24. Glycosaminoglycans (GAGs) quantification assay*

The amount of GAGs was quantified using the Blyscan Glycosaminoglycan Assay of the digested sample. 50 µL of the sample was mixed with 0.5 mL of Blyscan dye reagent and incubated at room temperature for 30 min in a shaker. The samples were spun down at 12000 rpm for 10 min. The supernatant was discarded and 0.25 mL of dissociation reagent added. Finally, the samples were vortexed, centrifuged at 12000 rpm for 5 min to remove the foam, and 100 µL were added to a 96-well plate. The absorbance was measured at 656 nm.

*2.2.25. Osteochondral explants*

Osteochondral explants were harvested from bovine stifle joints of 3- to 5-months-old calves, obtained from a local abattoir (Angst AG, Zurich, CH). Osteochondral plugs were drilled, cleaned and collected for culture.

*2.2.26. Statistical analyses*

All statistical analyses were performed in GraphPad Prism version 9. One-way or two-way ANOVA with Tukey's multi comparison test were used to analyze the data. A level of $p < 0.05$ was considered significant. All results were reported as mean ± standard deviation.

## 3. Results and discussion

*3.1. Fabrication and characterisation of granular hydrogels*

The design of an injectable, highly porous, and *in situ* crosslinkable material is of utmost importance for achieving a one-step medical procedure for articular cartilage repair. We designed the granular hydrogel by double-modifying HA: methacrylate groups to achieve the primary cross-linking (to form the microgels) and addition of TG-sensitive peptides for the secondary cross-linking (to anneal the microgels) [53].

HA was modified with methacrylic anhydride [47]; the addition of 20 equivalents of methacrylic anhydride to HA corresponded to a DS of ~ 30% (**Fig. S1**). The addition of methacrylate groups could be observed by FTIR spectroscopy by the appearance of a peak at ~1708–1712 $cm^{-1}$ corresponding to the C=O ester bond in the methacrylate group added to the HA backbone (**Fig. S2**) [54]. The compressive modulus was 11 kPa, and the degree of swelling 100%. Bulk hydrogels prepared from HAMA of 30% DS were mechanically pressed through a grid of 150 µm (large)- and 20 µm (small)- diameter pores three times, resulting in injectable (Fig. 2A top) microgels of 144 ± 94 µm, and 48 ± 20 µm in diameter (Fig. 2A bottom, 2B). The two sizes were selected because small microgels present a higher number of paths to allow cell infiltration, but bigger microgels instead present larger continuous 2D surfaces, which could also enhance cell migration. Once the microgel slurry was obtained, the microgels were functionalised with TG-K/RGD-K and TG-Q. Upon addition of thrombin (Thr)-activated FXIII to the granular hydrogel mix, crosslinking onsets immediately indicating the successful peptide grafting to the microgels. The granular hydrogels reached 3924 ± 210 Pa and 3156 ± 68 Pa in storage modulus for 20 µm and 150 µm sized granular hydrogels, respectively (Fig. 2C). The storage values were similar to the ones obtained by Muir et, al. when preparing granular hydrogels by extrusion fragmentation, around 3000 Pa [55]. However, their void fraction was much lower at around 8%, indicating that the methods for jamming and crosslinking the microgels provoke significant differences in their physical properties. Furthermore, to prove the TG-K peptide functionalization to single HAMA chains via Michael addition (between the cysteine thiols of the peptide and the methacrylate groups of the HAMA), we visualized by $^{1}H$ NMR the appearance of new peaks and the decrease in vinyl protons (**Fig. S3**). Also, photo-rheology showed the two possible cross-linking mechanisms (enzymatic and UV-light) of these double-functionalized macromonomers (**Fig. S4**).

The microgel slurry was cast in PDMS molds of 4 mm in diameter and 1 mm in height and cross-linked at 37 °C with Thr-activated FXIII for 30 min. While microgels without secondary annealing dispersed upon immersion in PBS, enzymatically cross-linked microgels remained stable (Fig. 2D, left). The granular hydrogels' morphology was evaluated by confocal microscopy (Fig. 2D, right), showing high void space ideal for cell proliferation and ECM deposition. Scanning electron microscopy (SEM) showed how hydrogels surface morphology changes when using granular systems. The surface is less uniform and composed of different microgels (**Fig. S5**).

As shown by Qazi et al., Blender can be a useful tool for evaluating pore interconnectivity within granular hydrogels [56]. Following their protocol, we simulated the displacement of an array of small beads and tracked their x, y, and z positions over 250 frames (Fig. 2E, Video S1, supporting information). Simulations predict improved pore interconnectivity with 20 µm-sized microgels based on differences in the tortuosity of bead trajectories and travel speed (Fig. 2E, top and bottom left). Using ImageJ, we were able to evaluate the porosity: granular hydrogels composed of 20 µm-sized microgels presented a smaller total void space (29 ± 3 %) when compared to 150 µm-sized microgels (36 ± 5 %) (Fig. 2F). Thus, even though 150 µm-sized microgels led to higher void space, they did not correlate with higher interconnectivity (lower bead path tortuosity). We therefore hypothesised that cells would colonise faster in hydrogels composed of 20 µm-sized microgels.

We next evaluated the mechanical properties and stability of the generated granular hydrogels. Compression tests revealed an inverse correlation between the elastic modulus and the total void space, with E = 8.5 ± 2.3 kPa and 6.5 ± 0.8 kPa for 20 µm and 150 µm-sized hydrogels using HAMA compared to 11.8 ± 1.4 kPa for bulk gels (Fig. 2G). When immersed in a hyaluronidase 10 U/mL solution at 37°C, secondary cross-linked microgels showed complete degradation after 4 days. Note that the degradation rate was not affected when comparing granular vs bulk hydrogels, which might be due to the high weight/volume ratio of microgel slurry (6% weight/volume) needed for the secondary annealing (Fig. 2H). In summary, HAMA microgels formed moldable and stable annealed structures with tunable porosity and interconnectivity as a function of microgel size, which allows for fast cell colonization. The summary of the granular hydrogels' properties when sized with different meshes can be found in Table S1.

*3.2. Evaluation of cell migration in granular hydrogels*

The first step towards endogenous repair is cell migration, so we encapsulated aggregates of 750 hBMSCs within the bulk and granular hydrogels to evaluate cell colonization. We studied three different parameters that can influence cell migration: (i) microgel size, (ii) incorporation adhesion peptides (RGD) on the TG sequence, and (iii) the presence of PDGF-BB (100 ng/mL) in the media. Additionally, as a positive control, we used a small amount of fibrin (Fib) (2 µg/mL) mixed into the microgels to promote cell migration. The different systems were evaluated after four days of culture; a projection of 100 µm z-stack (Fig. 3A) was analysed with a Python script, and two parameters were quantified: sprout length (Fig. 3B, left) and sprout number (Fig. 3B, right). From Fig. 3A it was observed that RGD and PDGF-BB increase considerably sprout length and sprout number achieving similar values as Fib containing hydrogels. As was also observed in Muir et al., the sprout length increased considerably when RGD was incorporated, which plays a major role in cell adhesion and migration [57]. Therefore,

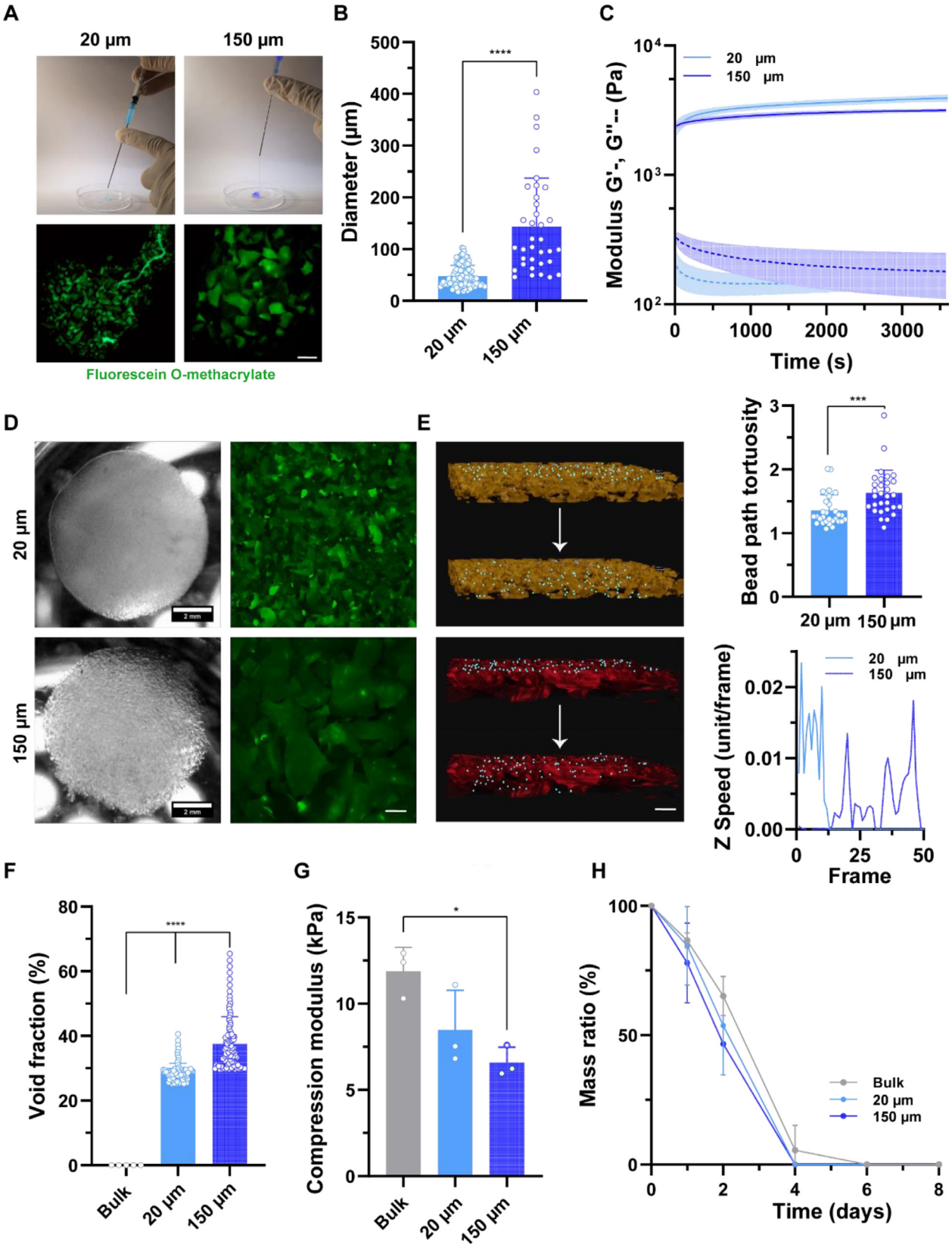


**Fig. 2.** Characterization of granular hydrogels. A) Images of granular hydrogels' injectability (top) and confocal images of HAMA microgels after being sized with the two different grids (bottom). Fluorescein O-methacrylate was incorporated into the resin mixture for visualization purposes. Scale bar 100 µm. B) Average diameter after sizing. C) Cross-linking of granular hydrogels sized with a 20 µm or 150 µm mesh. D) Optical images of granular hydrogels after being enzymatically cross-linked (left) and confocal image of cross-linked microgels (right). Scale bar 1 mm and 50 µm, respectively. E) Simulations with Blender for 20 µm-sized microgels (top, left) and 150 µm-sized microgels (bottom, left), granular hydrogels, bead-predicted path tortuosity (top, right) and travel speed (bottom, right). Scale bar 100 µm. F) Void fraction present in the cross-linked granular hydrogels. G) Compression modulus of the gels after being sized and secondary cross-linked. H) Degradation rate of differently sized granular hydrogels with hyaluronidase. Data are represented as mean ± standard deviation. Statistical significance was determined using one-way ANOVA with a Tukey's multiple comparisons test ($*p < .05$, $**p < .01$, $***p < .001$, and $****p < .0001$).

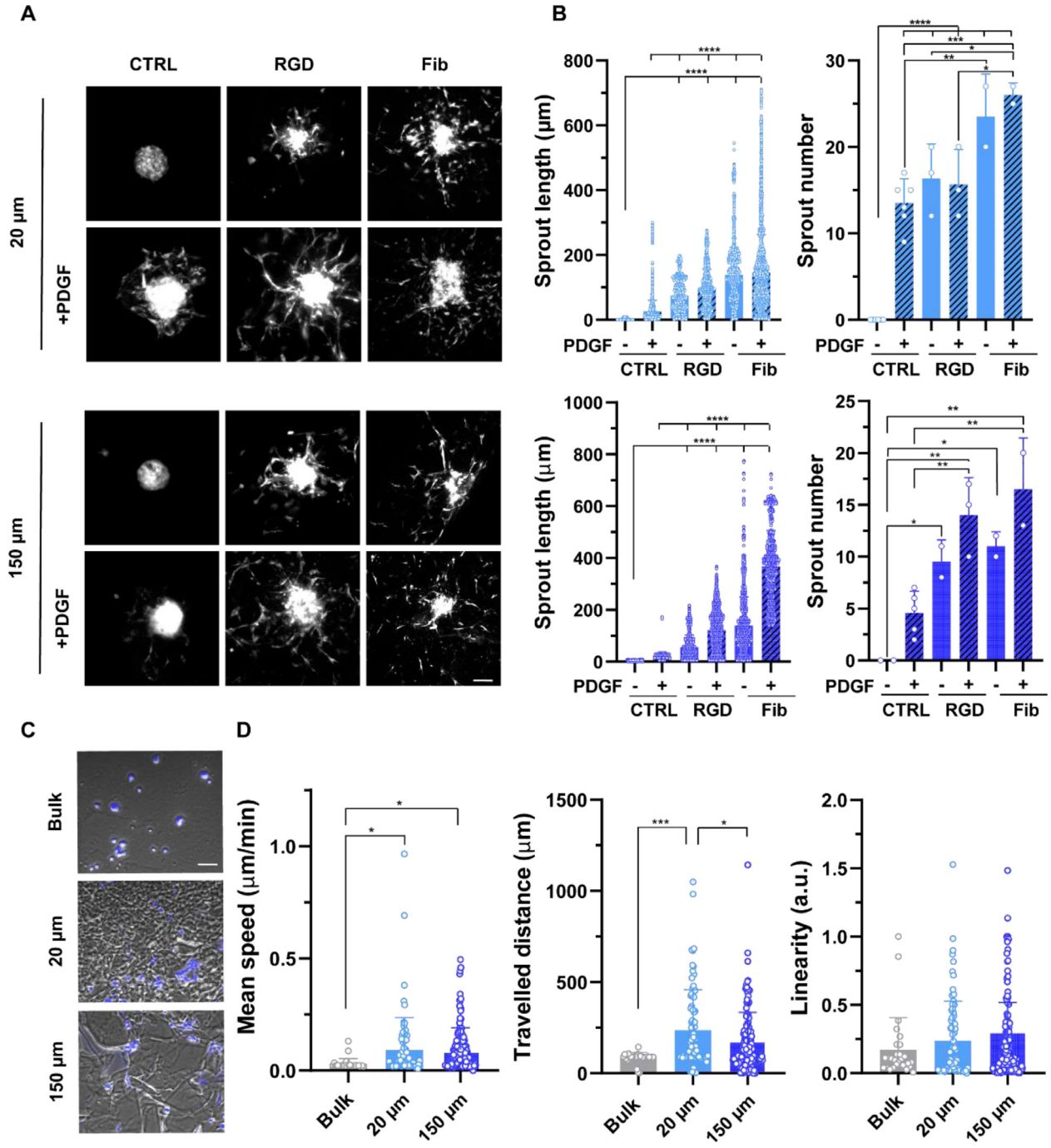


**Fig. 3.** *In vitro* hBMSC spheroids sprouting in granular hydrogels in the presence of RGD and PDGF-BB (100 ng/mL); these factors induce a similar sprouting to fibrin (Fib). A) Spheroids consisting of 750 hBMSCs in granular HAMA hydrogel (20 µm- and 150 µm-sized hydrogels) cultured for 4 days in the presence of RGD, PDGF, combined or with Fib. Scale bar = 100 µm. The images were used to quantify B) Sprout length (right) and sprout number (left) for 20 µm- (top) and 150 µm (bottom)-sized granular hydrogels. C) Microscope images of cells seeded in ibidi chambers. D) Mean speed, travelled distance and linearity of cells migrating in bulk, 20 µm-, and 150 µm-sized granular hydrogels containing RGD and PDGF in the media. Scale bar = 100 µm. Data are represented as mean ± standard deviation. Statistical significance was determined using a two- and one-way ANOVA with a Tukey's multiple comparisons test ($*p < .05$, $**p < .01$, $***p < .001$, and $****p < .0001$).

from this point on we used only granular hydrogels containing the TG-RGD-K peptide. The same behaviour was noted in the presence of PDGF-BB, but to a lesser extent [58]. Interestingly, when both PDGF-BB and RGD were present, the migration effect increased, demonstrating a synergistic influence and reaching similar values as the ones obtained with Fib, our positive control (Fig. 3B, left). Furthermore, no migration was observed when spheroids were encapsulated within bulk hydrogels (**Fig. S6**). Thus, our data suggest that when using granular hydrogels, RGD and PDGF-BB are necessary for maximising the mobility and the recruitment of hBMSCs and for avoiding the addition of Fib (which normally leads to the formation of fibrocartilage) to the healing cartilage. The similar migration behaviour was observed with 20 µm- and 150 µm-sized microgels. Significant differences between the microgel sizes were only observed when counting the number of sprouts, which was higher with 20 µm-sized microgels (Fig. 3B, right). This suggests

that having 150 μm-sized microgels limits the number of available paths for the cells to infiltrate, corroborating the results obtained from the tortuosity analysis.

To further investigate cell migration on granular hydrogels *vs* bulk gels, we used time-lapse microscopy on chemotactic chambers from Ibidi. A small amount of gel precursors mixed with hBMSCs (fluorescently labelled with CellTracker) were added to the middle chamber. To the left chamber, medium containing PDGF-BB (100 ng/mL) was added, and on the right, medium without PDGF-BB. Images were taken every 15 min for 72 h (Fig. 3C and Videos S2a, S2b and S2c). Using ImageJ and TrackMate plugin, it was possible to determine average speed, total distance and linearity. Considerable differences were observed between cell culture in 2D vs 3D. Cells displayed a significantly lower speed in 3D bulk gels than on 2D flat substrates (0.03 ± 0.02 μm/s and 0.59 ± 0.16 μm/s, respectively). Accordingly, the total distance travelled was smaller in bulk gels, 85 ± 28 μm, compared to 2D flat substrates, 746 ± 499 μm. When comparing the linearity, the ratio between the mean straight-line speed and the track mean speed, we found that the difference is much lower: 0.19 ± 0.27 for 2D flat surfaces and 0.17 ± 0.23 for bulk hydrogels. Instead, when using granular hydrogels, either 20 μm- or 150 μm-sized microgels, we could increase the values of average speed (0.09 ± 0.14 and 0.09 ± 0.09 μm/s), total distance (237± 221 μm and 1678 ± 167 μm), and linearity (0.23 ± 0.29 and 0.23 ± 0.28), bringing them closer to the ones obtained in 2D. Also, a slight increase in linearity was observed, which could be related to the presence of more constrained paths (Fig. 3D) [59]. Cells encapsulated in bulk hydrogels have their motility constrained if no degradable moieties exist. As already shown by F. Anjum et al., cell migration in bulk gels is enhanced in the presence of RGD and, most importantly, when the gels contain matrix metalloproteinase-sensitive domains [60]. Instead, in granular hydrogels, there is enough void space where the cells can easily infiltrate without the need for matrix degradation [61].

### 3.3. Design of heterogeneous granular hydrogels

As shown previously, the addition of PDGF-BB is crucial to achieving good cell infiltration. The efficient retention of GFs could prevent undesired side effects, burst release, and the need for multiple injections, besides increasing GFs' half-life time. Therefore, mimicking nature, we modified HA to generate sulfate groups for retaining GFs and slowly releasing them. HAMA was grafted with sulfate groups following the protocol of Feng et. al. FTIR spectroscopy of SHAMA exhibited two absorption bands at 1240 and 820 $cm^{-1}$, due to the S=O asymmetric stretching and S-O-C symmetrical stretching, respectively, and thereby confirmed the successful sulfation of the polymer (**Fig. S7**) [35,36]. The sulfation reaction led to a final atomic sulfur content of 7%, as shown by elemental analysis, corresponding to a degree of sulfation of 1.32. After the addition of the sulfate groups, the physical properties of the polymer changed. These changes include a shortening of the polymer chains, an increase in hydrophilicity (showing a higher swelling ratio), and the increase of steric hindrance, which reduces enzymatic degradation.

We therefore selected a mixture of SHAMA and HAMA polymers containing just enough negatively charged groups to convey GFs' retention and cell-homing properties without altering the physical properties of the microgels. Bulk gels containing two different percentages of SHAMA, 25% and 50%, were therefore evaluated. To confirm the successful incorporation of SHAMA, energy-dispersive X-ray spectroscopy (EDX) was conducted to detect sulfur (S) atoms (**Fig. S8**). Results showed an even distribution of S element in the bulk gels, indicating that SHAMA was well mixed and retained in the hydrogels.

Swelling ratios showed that HAMA hydrogels did not swell, whereas SHAMA hydrogels did undergo minimal swelling (1.25 and 1.35 over 24 h for 25% SHAMA and 50% SHAMA, respectively) (Fig. 4A). Diffusion coefficients of FITC-labelled dextran probes (with molecular weights of 10 and 500 kDa) entrapped in the different hydrogel formulations were studied by FRAP (Fig. 4B). While 10 kDa (featuring a hydrodynamic diameter of ≈ 2.3) [62] diffused with good efficiency in all hydrogel conditions, the diffusion of 500 kDa (featuring a hydrodynamic diameter of ≈ 30.6 nm) [63] was mostly restricted. 50% SHAMA hydrogels displayed significantly higher diffusion coefficients compared to HAMA hydrogels, indicating that the pore size of pure HAMA is slightly smaller than 50% SHAMA. However, no significant differences were observed between HAMA and 25% SHAMA. Also, the storage moduli of all hybrid hydrogels remained within the range of 800 to 1200 Pa, with SHAMA 50% being in the softer range (**Fig. S9**).

The biological interaction between hBMSCs and the different materials was evaluated by incubating 20 μm-sized microgels made of HAMA, 25% SHAMA and 50% SHAMA with hBMSCs for 48 h and Live Dead stained (Fig. 4C). The cells surrounding HAMA microgels were fibroblastic in appearance, and they spread in the plastic culture plate. Surprisingly, the cells surrounding SHAMA microgels covered the entire microgel surface. The high cell attachment to un-loaded SHAMA microgels could be due to the retention of proteins and GFs present in the cell culture medium. This attachment was independent of SHAMA percentage, indicating that 25% is enough to exert an effect on cells without significantly changing the physical properties of the hydrogels.

Therefore, 25% SHAMA microgels were used as GFs microislands to guide the recruitment of BMSCs and chondrocytes. A one-to-one ratio of 25% SHAMA (Rhodamine labelled) microgels and HAMA microgels (FITC labelled) were mixed to form heterogenous granular hydrogels (Fig. 4D). For 20 μm-sized microgels, the volume distribution is 42% HAMA, 34% of 25% SHAMA, and 21% void, and for 150 μm-sized microgels it is 27% HAMA, 28% of 25% SHAMA, and 45% void. Again, the void space is higher for 150 μm-sized microgels due to the highly irregular shape that makes it more difficult for the microgels to be tightly packed.

### 3.4. Chondrogenesis in heterogeneous granular hydrogels

To achieve chondral endogenous repair, we need chemical cues to stimulate cell migration but also chondrogenesis. Therefore, we sought to characterize the capacity of granular hydrogels to promote cartilaginous matrix deposition by hBMSCs with and without sulfated microislands in the presence of TGF$\beta$-3 in the cell culture medium. hBMSCs were encapsulated at 10 M cells/mL concentration in bulk, 20 μm- and 150 μm-sized hydrogels and cultured for 3 weeks in chondrogenic media. In all cases, viabilities were higher than 85% after 3 weeks, indicating no cytotoxicity derived from the prepared materials (Fig. 4E and F). In bulk hydrogels, strong pericellular, but not homogenous, deposition of proteins and GAGs was observed (Fig. 4E). Instead, tissue maturation was enhanced and more homogeneous for the microgel-based scaffolds [52]. This indicated that void space is favourable for matrix cell deposition. However, both types of collagen were present in all systems independently of the microgel size or composition. The main differences were found on the distribution of Collagen II, presenting zones with higher intensity when heterogenous granular hydrogels were used. Instead, the production of GAGs was not affected when incorporating sulfated microgels. Negative controls are shown in **Fig. S10**.

Complementary to the analysis of tissue composition, biomechanical properties have been considered an essential parameter for evaluating the quality of the generated cartilage tissue. An increase in compressive modulus was observed after 21 days of

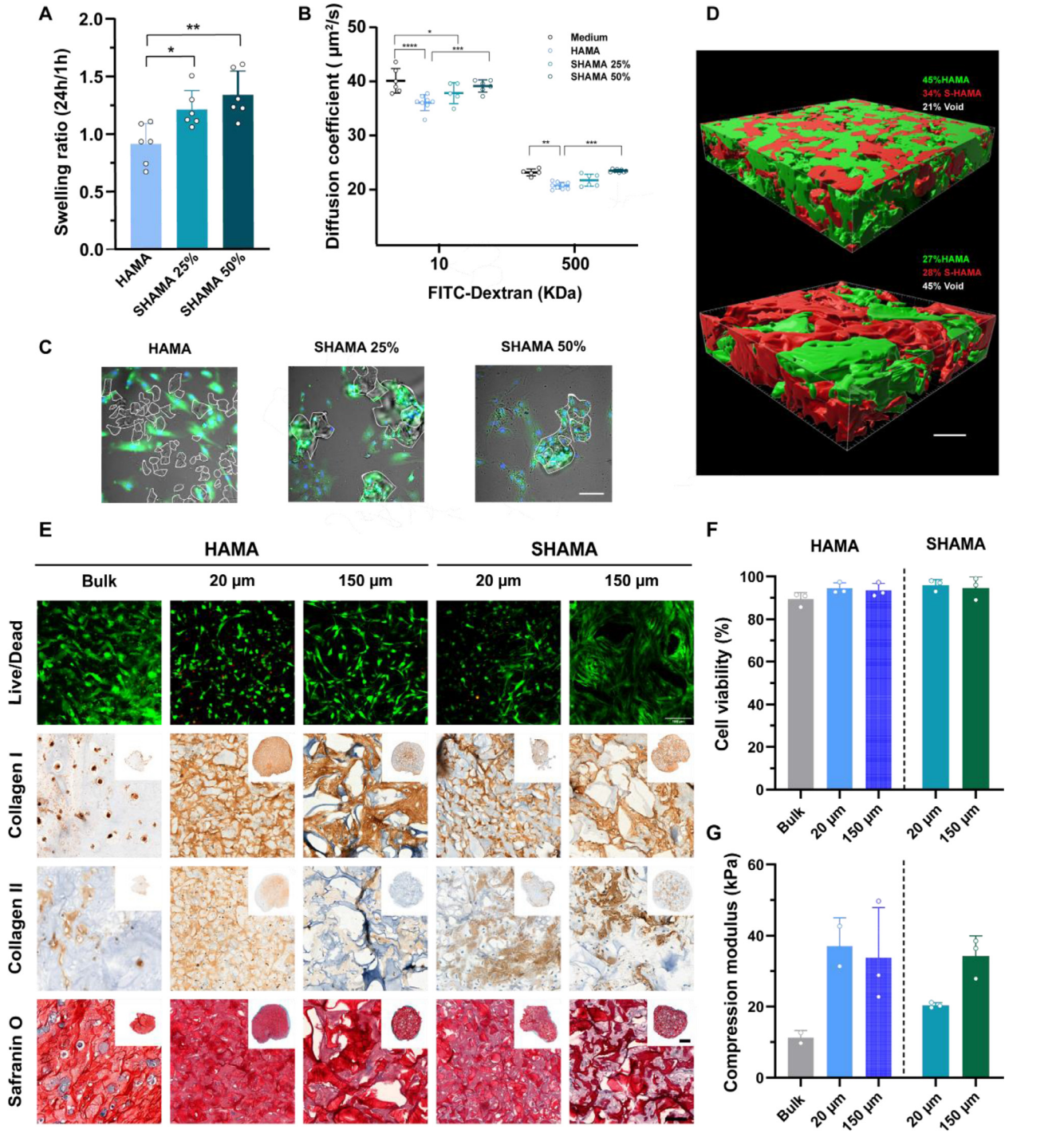


**Fig. 4.** Physical characterization of SHAMA bulk hydrogels and chondrogenic evaluation of homogenous and heterogenous granular hydrogels. A) Swelling ratio of HAMA, 25% SHAMA, and 50% SHAMA bulk hydrogels. B) Diffusion coefficient of different MW FITC-Dextran in HAMA, 25% SHAMA and 50% SHAMA bulk hydrogels. C) Cell attachment to 20 μm-sized microgels composed of HAMA, 25% SHAMA, and 50% SHAMA; microgels' contour is colored in white, scale bar = 50 μm. D) 3D reconstruction of the heterogenous gels prepared by sizing with the 20 μm (top) or 150 μm (bottom) grid, scale bar = 50 μm. E) Chondrogenic analysis of hBMSCs encapsulated within hydrogels with different architectures (bulk, 20 μm-, and 150 μm-sized granular hydrogels) and different chemical composition (HAMA and 25% SHAMA). Live/dead immunofluorescence and histological analysis showing collagen I, collagen II and glycosaminoglycans (Safranin O). Scale bar = 100 μm and 1 mm inset. F) Live/dead quantification. G) Compression modulus of the constructs after 3 weeks of culture. Data are represented as mean ± standard deviation. Statistical significance was determined using one-way ANOVA with a Tukey's multiple comparisons test ($*p < .05$, $**p < .01$, $***p < .001$, and $****p < .0001$).

culture, 13 ± 3 kPa, 37 ± 8 kPa, and 34 ± 14 kPa for bulk, 20 μm- and 150 μm-sized hydrogels of HAMA composition. As expected, granular hydrogels promoted better tissue maturation: these results are in accordance with the data shown by Li et al., achieving a compressive modulus of 16 ± 1 kPa for the bulk hydrogel and 19 kPa ± 1 kPa for the PEG-succinimidyl glutaramide-assembled microgels when hBMSCs were encapsulated and cultured for 21 days [64]. The compressive modulus with either 20 μm- or 150 μm-sized hydrogels in the presence of 25% SHAMA microgels was slightly lower than with HAMA but still in the range of 20-40 kPa, as previously found for hBMSCs culture (Fig. 4G). Overall, we can say that granular hydrogels perform better than bulk gels in

achieving cartilage; and hydrogels containing sulfated microislands can promote chondrogenesis of hBMSCs and are more effective in terms of localized collagen II production.

### 3.5. Guiding cell migration in heterogeneous granular hydrogels

Previous results suggested that PDGF-BB and TGF$\beta$-3 are crucial in stimulating cell migration and chondrogenesis; for that reason, we encapsulated both GFs into 25% SHAMA microgels [42]. Both TGF$\beta$-3 and PDGF-BB have high isoelectric points (8.3 and 9.8, respectively), making them positively charged at a neutral pH [65]. Their positive charges will interact with the negatively charged sulfate groups present in SHAMA microgels.

To validate our hypothesis that sulfated microislands (red microgels) can sequester and provoke GF gradient distributions in a tissue-like environment, we swelled the lyophilized 25% SHAMA

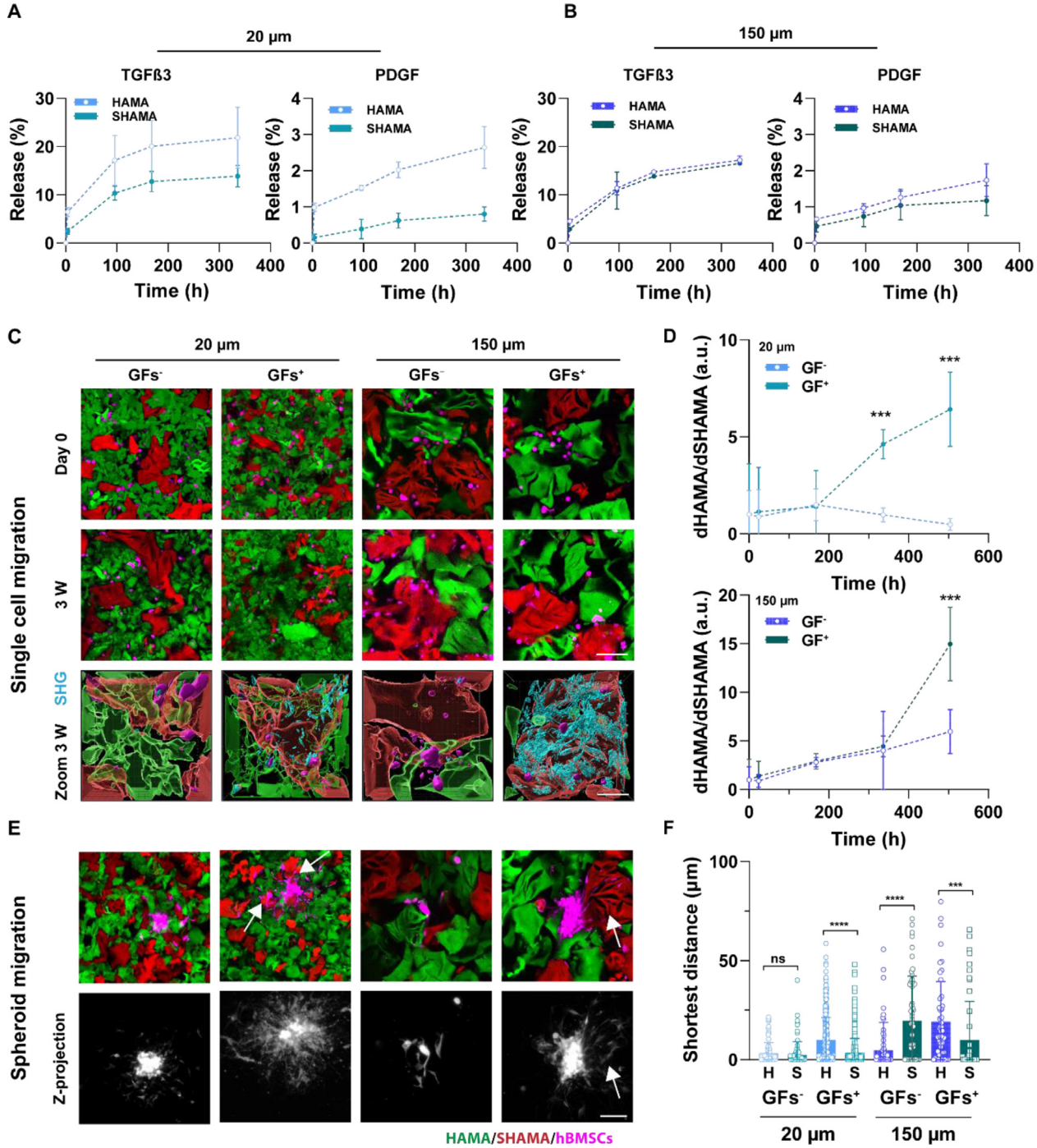


**Fig. 5.** Sulfated microislands in heterogenous gels promote cell migration and recruitment. Release curves of TGF-$\beta$3 (left) and PDGF-BB (right) from HAMA (empty symbols) and SHAMA (filled symbols) systems when 20 µm-(A) or 150 µm-(B) sized microgels are employed. C) Confocal images of cells labelled with CellTracker Deep Red embedded on different systems at day 0 (top), after 3 weeks (middle) and 3D reconstruction after 3 weeks incorporating the SHG signal indicator of collagen production (bottom). Scale bar 100 and 50 µm, respectively. D) Ratio of the shortest distance (d) to HAMA vs the shortest distance to SHAMA with ($^+$) and without ($^-$) GFs incorporated over time, 20 µm sized microgels (top) 150 µm sized microgels (bottom). E) Spheroid migration assay after 4 days of culture. Scale bar 100 µm. F) Cell shortest distance calculation towards HAMA (H) or SHAMA (S) microgels. Data are represented as mean ± standard deviation. Statistical significance was determined using one and two-way ANOVA with a Tukey's multiple comparisons test ($*p < .05$, $**p < .01$, $***p < .001$, and $****p < .0001$).

and HAMA (as controls) microgels in TRIS buffer containing GFs. The GF release was evaluated for 2 weeks by ELISA assays (Fig. 5A and B). Less than 20% and 2% of encapsulated TGF$\beta$-3 and PDGF-BB were released in 20 μm-sized hydrogels containing SHAMA microgels; instead, for purely HAMA granular hydrogels, the release was faster. However, this effect could not be established for 150 μm-sized hydrogels. Therefore, we conclude that: (1) the release is slower with the presence of SHAMA microgels in 20 μm-sized hydrogels; (2) the release of PDGF-BB is lower than TGF$\beta$-3 because of its higher isoelectric point; and (3) the release is faster in 20 μm-sized hydrogels because of the higher surface area-to-volume ratio.

Once the GFs' retention was validated, we evaluated the direction of cell migration on these heterogeneous granular hydrogels. Cells were labelled with CellTracker Deep Red, and two different setups were evaluated: (1) single cell migration and (2) sprout outgrowth from spheroids (Fig. 5C and E). For the single cell migration experiment, pictures were taken over a period of three weeks. At time point 0, the ratio between the different types of microgel and single cell distances (distance of each single cell to the nearest HAMA microgel (green) vs SHAMA microgel (red), **Figs. S11** and **S12**) was almost 1 in all granular hydrogel compositions, indicating a homogenous cell distribution. Interestingly, this ratio changed considerably over time, becoming higher than 1 af-

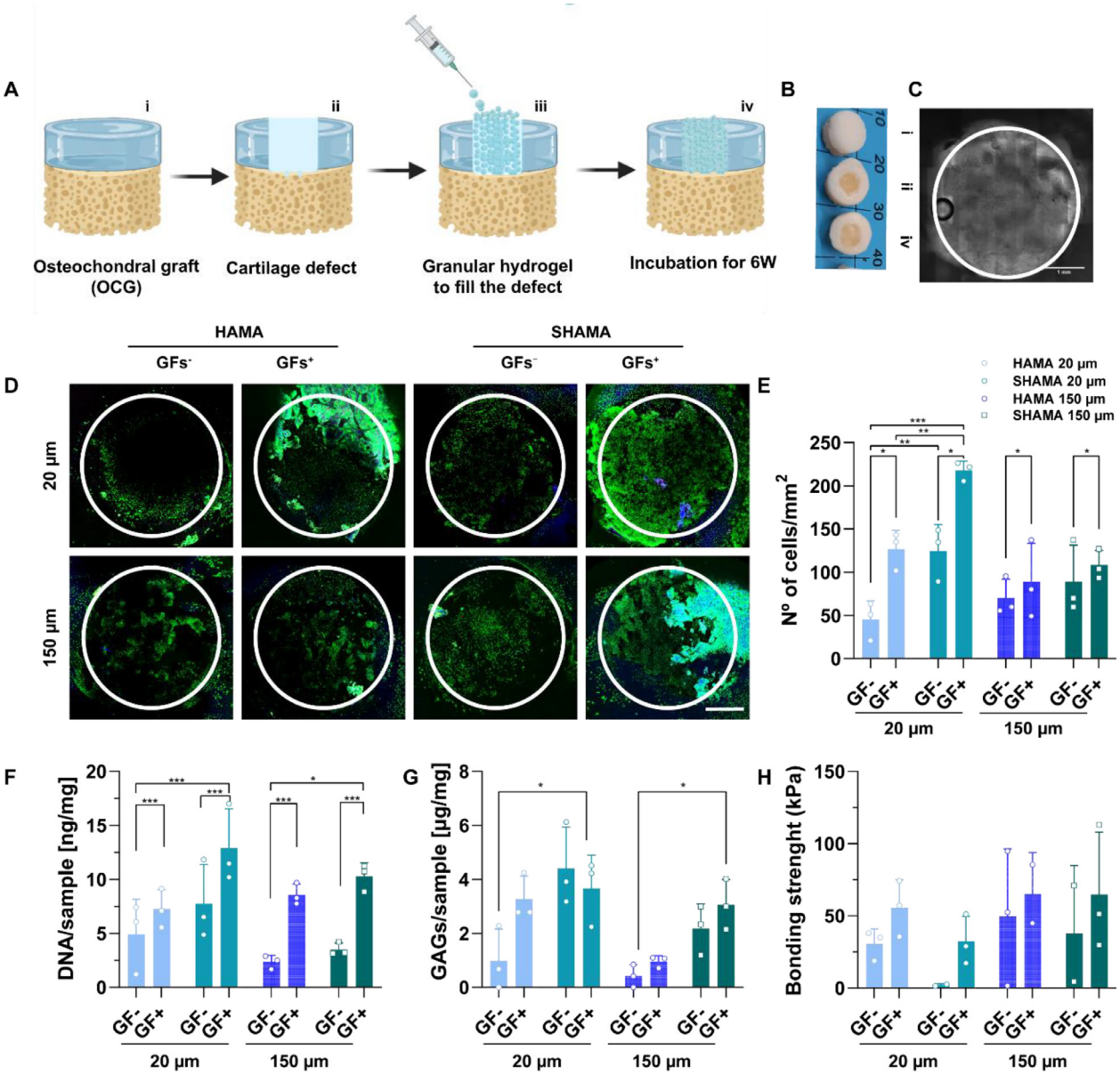


**Fig. 6.** Filling cartilage defects with granular hydrogels to promote cell recruitment and *de novo* cartilage formation *in vitro*. A) Procedure to prepare cartilage defects on OCG: (i) OCG are obtained from bovine knees from the slaughter house; plugs are obtained by using surgical mosaicplasty tools (7.4 in diameter and 6 mm in height); (ii) cartilage holes are obtained by using biopsy punchers of 4 mm in diameter, and four holes at 0.5 mm are made in the bone; (iii) the defect is filled with a granular hydrogel and (iv) incubated for 6 weeks (to promote migration and differentiation). B) Photographs of the plugs in steps i, ii, and iv. C) Optical image of the holes created on the plugs and filled with microgels. D) Live/Dead tiles scan of the filled defect after 6 weeks. E) Quantification of number of cells per mm$^2$. Scale bar: 1 mm. F) DNA quantification by the Pico-Green assay, and GAGs quantification by the DMMB assay (G), bonding strength between the gel and the cartilage measured by push-out tests (H). Data are represented as mean ± standard deviation. Statistical significance was determined using one-way ANOVA with a Tukey's multiple comparisons test ($*p < .05$, $**p < .01$, $***p < .001$, and $****p < .0001$).

ter just one week for both 20 μm- and 150 μm-sized hydrogels (cell distance to SHAMA becomes smaller than to HAMA). This phenomenon is significantly enhanced when GFs are encapsulated within the sulfated microgels (Fig. 5D). Also, we can observe differences between 20 μm- and 150 μm-sized hydrogels that could be correlated to the slower GF release in 150 μm-sized hydrogels. Overall, this demonstrates that cells can sense the sulfated microislands and migrate towards them. Another striking feature is that collagen production was more pronounced near the SHAMA microgels, as observed by second-harmonic generation (SHG) (Figs. 5C and **S13)**.

The same setup as in Fig. 3 was used to analyse the direction of the spheroids' sprouts after four days in culture (Fig. 5E). It is noteworthy that cell migration was significantly enhanced when GFs were encapsulated in SHAMA microgels, achieving similar values to when PDGF-BB was present in the cell culture medium (Fig. 3A). This proves again the GFs' encapsulation efficiency due to the sulfated microgels. The microgel size affected mainly the number of sprouts (higher for 20 μm sized microgels) and not the length of the sprouts. As previously seen, cell migration was directed towards SHAMA microgels (shorter distances of the cells towards SHAMA microgels) (Fig. 5F). In summary, these results suggest that cells can sense the GF hotspots in the heterogenous granular hydrogels, enhancing cell migration, collagen production, and proliferation in the surrounding areas without the need of soluble GFs in the medium.

### *3.6. 3.6 Bovine osteochondral explants to evaluate cell homing and chondrogenesis*

Finally, to evaluate chondrogenesis and cell migration simultaneously, we designed a relevant model for studying endogenous articular cartilage repair. Acellular heterogenous granular hydrogels were injected and *in situ* cross-linked into pre-made cartilage defects on bovine osteochondral explants (Fig. 6A, B and C). Importantly, no cells were added on the granular hydrogel and no GFs were present on the culture medium to better mimic the one-step medical procedure for articular cartilage repair. Bulk gels were also tested, but they detached from the osteochondral grafts after one week of culture, indicating poor integration, cell invasion and maturation. For that reason, they were not included in this study. Interestingly, all granular hydrogel conditions showed high cell invasion compared to bulk gels and were retained inside the defect during the culture period. Live/Dead staining was performed to evaluate cell viability and number of cells per area of defect (cells/mm$^2$) (Fig. 6D). Interestingly, the cellularity of the samples

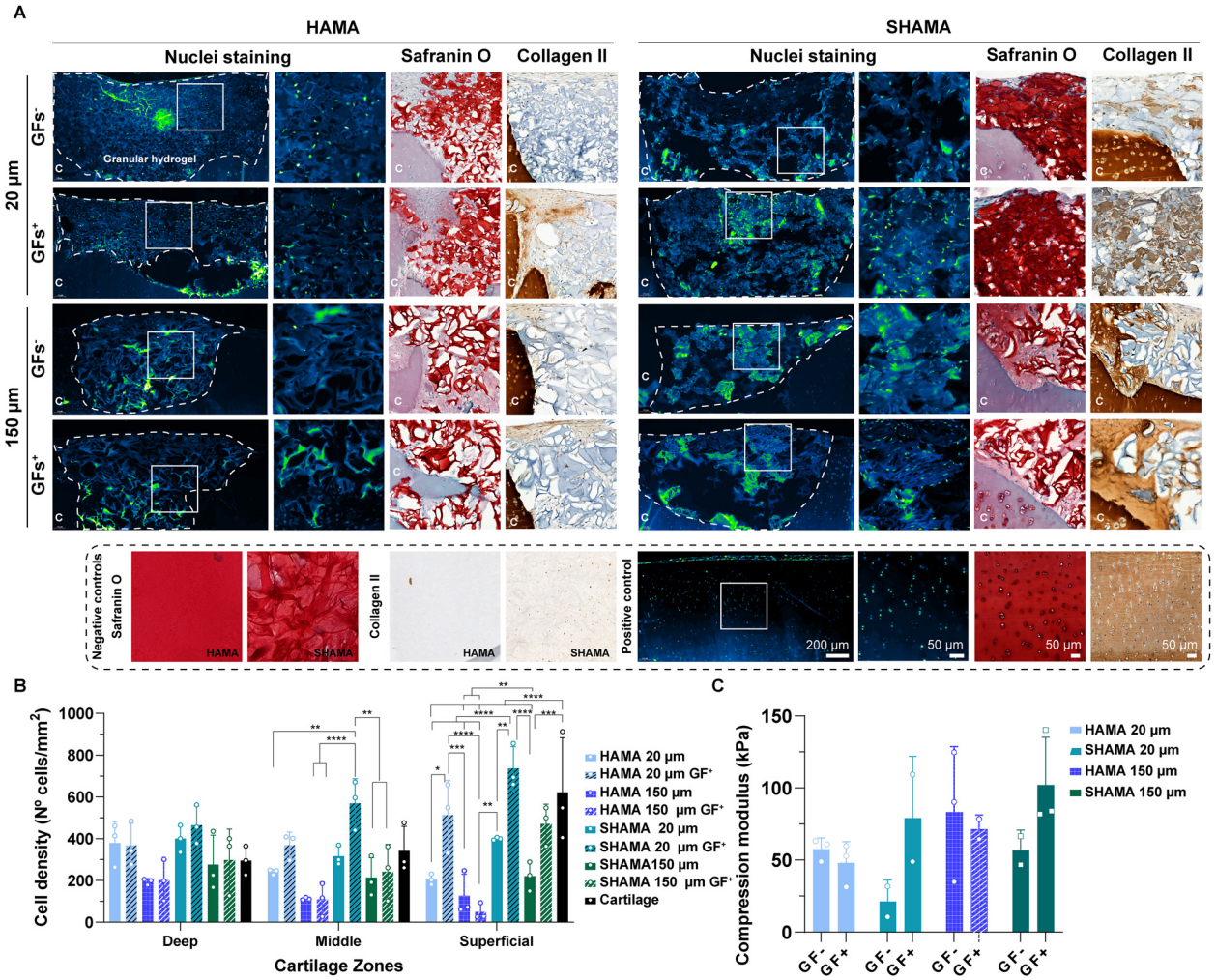


**Fig. 7.** A) Histological and immunohistological staining's of osteochondral graft filled with granular hydrogels for nuclei staining (Hoechst), GAGs (Safranin O), and collagen II. B) Quantification of cell density in three different cartilage zones (Deep, Middle and Superficial). Stripped bars represent the presence of GF. C) Compression modulus of the hydrogels cultured on the osteochondral graft after 6 weeks of culture. Data are represented as mean ± standard deviation. Statistical significance was determined using two-way ANOVA with a Tukey's multiple comparisons test ($*p < .05$, $**p < .01$, $***p < .001$, and $****p < .0001$).

(Fig. 6E) was very high when GFs were incorporated and significantly enhanced when the sulfated microislands were present (with or without GF). Also, it was noticed that 20 µm-sized hydrogels showed better cell infiltration, even though, as previously mentioned, the void space is smaller, which indicates that void interconnectivity is a very important parameter in allowing for cell colonization. Sulfated microislands without incorporated GFs were already able to exert an impact on cell migration, which could indicate that sulfated microgels can retain GFs synthesised by the cells nearby and therefore continue to promote cell migration and proliferation. DNA content per gel mass confirmed this hypothesis (Fig. 6F). As expected, again, with 20 µm-sized hydrogels and the presence of GFs, the DNA content was higher. Later, the presence of GAGs per granular hydrogel was quantified. As seen in Fig. 6G, the number of GAGs was higher in sulfated microgels after normalization with the signal from empty gels. The production of GAGs corrected by the amount of DNA resulted in no significant differences between the two groups. This could indicate that a longer period would be needed to properly evaluate tissue maturation.

The next step was to elucidate the integration of the injected material with the host tissue. Previously, the adhesion of HA-TG was tested in cartilage explant showing a bonding strength of 2 kPa without any culture time [66]. Here, even though our material is comprised of a granular substance, after 6 weeks of culture we achieved 20-50 kPa of bonding strength – quite a lot for a granular hydrogel instead of a bulk gel. These results confirmed that granular hydrogels induce cell homing and production of ECM, which in turn integrates with the material to the host tissue (Fig. 6H). The most significant difference seen when comparing the different materials with and without the incorporation of GFs was the consistently higher values reached with GFs.

The histological and immunohistological analysis confirmed that cell infiltration and tissue development in both materials (HAMA and SHAMA) is possible even without GFs in the medium (Fig. 7A). A cellular network and ECM between the microgels could be seen after 6 weeks. Hoechst staining (shown in green) presented higher cellularity in the superficial zone of the cartilage defect (Fig. 7B) and significantly enhanced when using 20 µm-sized hydrogels with sulfated microislands. Cartilage-like matrix composition of glycosaminoglycans (GAGs, Safranin O) and collagen II increased in intensity in the histological sections after culture. Collagen II staining was stronger in the SHAMA systems compared to HAMA. From the histological sections, we could observe that cells mostly come from the bottom (MSCs from the subchondral bone) and top (cartilage surface that contains the biggest amount of chondroprogenitor cells). Again, bigger microgels presented less cell infiltration and tissue maturation. In conclusion, 20 µm-sized hydrogels containing loaded sulfated microislands showed higher cell infiltration, collagen II and GAG content. Regarding the mechanical properties of the granular gels, when GFs were incorporated into the materials, the stiffness increased to 20-100 kPa, which was considerably higher than the initial stiffness of around 10 kPa (Fig. 7C).

Altogether, these results confirmed the biocompatibility of HAMA and SHAMA microgels and demonstrated that granular materials can promote endogenous cartilage repair characterized by high cell infiltration, mechanical stiffening over time, and cartilage-like ECM deposition. Also, as expected, the addition of GFs is beneficial for cartilage matrix production and is even more significant in the presence of sulfated microislands, mainly in terms of cellularity and collagen II production. This technology can provide a possible one-step procedure for cartilage lesion repair, facilitating the treatment of chondral lesions without the need of autologous cells and the proper retention of GFs. Therefore, this can reduce overall procedure costs and time.

## 4. Conclusion

We developed an injectable, *in situ* cross-linkable heterogeneous granular hydrogel containing non-covalently bound GFs. Despite cartilage's low capacity for self-repair, we achieved a prominent endogenous response by injecting the heterogeneous granular hydrogel to the chondral defect. Many cells colonised the hydrogel and produced cartilage ECM making the gels stiffer and increasing the bonding strength of the granular hydrogel with the host tissue.

The most promising results were obtained when using 20 µm-sized hydrogels, presenting a higher void interconnectivity and containing the GFs loaded sulfated microislands. These results have potential for developing cell-free injectables to treat articular cartilage defects, avoiding the use of expensive cell-based therapies. For a faster translational product, the gel could be loaded with patient platelet lysate instead of commercial GFs. Because of its simplicity, high void space, and modularity, we can foresee loading the hydrogels with various GFs cocktails, to recruit different types of cells and promote the repair of diverse tissues.

## Declaration of Competing Interest

The authors declare that they have no known competing financial interests or personal relationships that could have appeared to influence the work reported in this paper.

## Acknowledgments

The authors would like to thank the European Commission for providing financial support with the MSCA individual fellowship (Grant no: 885797) for AP and Swiss National Science Foundation (No. 192656) for MZ. Thanks also to the ScopeM centre at ETH for providing technical support, David Fercher for the peptide synthesis and Eduard Bermejo for helping in the image analysis.

## Supplementary materials

Supplementary material associated with this article can be found, in the online version, at doi:10.1016/j.actbio.2023.03.045.

## References

[1] A.R. Martín, J.M. Patel, H.M. Zlotnick, J.L. Carey, R.L. Mauck, Emerging therapies for cartilage regeneration in currently excluded 'red knee' populations, Npj Regen. Med. 4 (2019) 1–12.
[2] T. Ramos, L. Moroni, Tissue engineering and regenerative medicine 2019: the role of biofabrication - a year in Review, Tissue Eng. - Part C Methods 26 (2020) 91–106.
[3] X. Hu, Y. Wang, Y. Tan, J. Wang, H. Liu, Y. Wang, S. Yang, M. Shi, S. Zhao, Y. Zhang, Q. Yuan, A difunctional regeneration scaffold for knee repair based on aptamer-directed cell recruitment, Adv. Mater. 29 (2017) 1605235.
[4] X. Sun, H. Yin, Y. Wang, J. Lu, X. Shen, C. Lu, H. Tang, H. Meng, S. Yang, W. Yu, Y. Zhu, Q. Guo, A. Wang, W. Xu, S. Liu, S. Lu, X. Wang, J. Peng, In situ articular cartilage regeneration through endogenous reparative cell homing using a functional bone marrow-specific scaffolding system, ACS Appl. Mater. Interfaces. 10 (2018) 38715–38728.
[5] A. Lolli, K. Sivasubramaniyan, M.L. Vainieri, J. Oieni, N. Kops, A. Yayon, G.J.V.M. van Osch, Hydrogel-based delivery of antimiR-221 enhances cartilage regeneration by endogenous cells, J. Control. Release. 309 (2019) 220–230.
[6] Z. Yang, H. Li, Y. Tian, L. Fu, C. Gao, T. Zhao, F. Cao, Z. Liao, Z. Yuan, S. Liu, Q. Guo, Biofunctionalized structure and ingredient mimicking scaffolds achieving recruitment and chondrogenesis for staged cartilage regeneration, Front. Cell Dev. Biol. 9 (2021) 1–17.
[7] Z. Li, H. Cao, Y. Xu, X. Li, X.W. Han, Y. Fan, Q. Jiang, Y. Sun, X. Zhang, Bioinspired polysaccharide hybrid hydrogel promoted recruitment and chondrogenic differentiation of bone marrow mesenchymal stem cells, Carbohydr. Polym. 267 (2021) 118224.
[8] Z. Yang, T. Zhao, C. Gao, F. Cao, H. Li, Z. Liao, L. Fu, P. Li, W. Chen, Z. Sun, S. Jiang, Z. Tian, G. Tian, K. Zha, T. Pan, X. Li, X. Sui, Z. Yuan, S. Liu, Q. Guo, 3D-Bioprinted difunctional scaffold for in situ cartilage regeneration based on aptamer-directed cell recruitment and growth factor-enhanced cell chondrogenesis, ACS Appl. Mater. Interfaces. 13 (2021) 23369–23383.

[9] C.H. Lee, J.L. Cook, A. Mendelson, E.K. Moioli, H. Yao, J.J. Mao, Regeneration of the articular surface of the rabbit synovial joint by cell homing: a proof of concept study, Lancet 376 (2010) 440–448.
[10] L. Hao, Z. Tianyuan, Y. Zhen, C. Fuyang, W. Jiang, Y. Zineng, D. Zhengang, L. Shuyun, H. Chunxiang, Y. Zhiguo, G. Quanyi, Biofabrication of cell-free dual drug-releasing biomimetic scaffolds for meniscal regeneration, Biofabrication 14 (2022) 015001.
[11] Y. Lu, Y. Wang, H. Zhang, Z. Tang, X. Cui, X. Li, J. Liang, Q. Wang, Y. Fan, X. Zhang, Solubilized cartilage ECM facilitates the recruitment and chondrogenesis of endogenous BMSCs in collagen scaffolds for enhancing microfracture treatment, ACS Appl. Mater. Interfaces. 13 (2021) 24553–24564.
[12] Z. Luo, L. Jiang, Y. Xu, H. Li, W. Xu, S. Wu, Y. Wang, Z. Tang, Y. Lv, L. Yang, Mechano growth factor (MGF) and transforming growth factor (TGF)-$\beta$3 functionalized silk scaffolds enhance articular hyaline cartilage regeneration in rabbit model, Biomaterials 52 (2015) 463–475.
[13] A.C. Daly, L. Riley, T. Segura, J.A. Burdick, Hydrogel microparticles for biomedical applications, Nat. Rev. Mater. 5 (2020) 20–43.
[14] D.R. Griffin, W.M. Weaver, P.O. Scumpia, D. Di Carlo, T. Segura, Accelerated wound healing by injectable microporous gel scaffolds assembled from annealed building blocks, Nat. Mater. 14 (2015) 737–744.
[15] N.J. Darling, E. Sideris, N. Hamada, S.T. Carmichael, T. Segura, Injectable and spatially patterned microporous annealed particle (MAP) hydrogels for tissue repair applications, Adv. Sci. 5 (2018) 1–8.
[16] Z. Ataie, S. Kheirabadi, J.W. Zhang, A. Kedzierski, C. Petrosky, R. Jiang, C. Vollberg, A. Sheikhi, Nanoengineered granular hydrogel bioinks with preserved interconnected microporosity for extrusion bioprinting, Small 18 (2022) 2202390.
[17] A.C. Suturin, A.J.D. Krüger, K. Neidig, N. Klos, N. Dolfen, M. Bund, R. Sebers, A. Manukanc, G. Yazdani, Y. Kittel, D. Rommel, J. Köhler, L. De Laporte, A.C. Suturin, A.J.D. Krüger, K. Neidig, N. Klos, N. Dolfen, M. Bund, T. Gronemann, R. Sebers, Annealing high aspect ratio microgels into macroporous 3D scaffolds allows for higher porosities and effective cell migration, Adv. Healthc. Mater. (2022) 2200989.
[18] J.M. de Rutte, J. Koh, D. Di Carlo, Scalable high-throughput production of modular microgels for in situ assembly of microporous tissue scaffolds, Adv. Funct. Mater. 29 (2019) 201900071.
[19] C.E. Miksch, N.P. Skillin, B.E. Kirkpatrick, G.K. Hach, V.V. Rao, T.J. White, K.S. Anseth, 4D Printing of extrudable and degradable poly(ethylene glycol) microgel scaffolds for multidimensional cell culture, Small 18 (2022) 2200951.
[20] T.H. Qazi, J.A. Burdick, Granular hydrogels for endogenous tissue repair, Biomater. Biosyst. 1 (2021) 100008.
[21] Q. Feng, D. Li, Q. Li, X. Cao, H. Dong, Microgel assembly: Fabrication, characteristics and application in tissue engineering and regenerative medicine, Bioact. Mater. 9 (2022) 105–119.
[22] J. Fang, J. Koh, Q. Fang, H. Qiu, M.M. Archang, M.M. Hasani-Sadrabadi, H. Miwa, X. Zhong, R. Sievers, D.W. Gao, R. Lee, D. Di Carlo, S. Li, Injectable drug-releasing microporous annealed particle scaffolds for treating myocardial infarction, Adv. Funct. Mater 30 (2020) 2004307.
[23] E. Sideris, S. Kioulaphides, K.L. Wilson, A. Yu, J. Chen, S.T. Carmichael, T. Segura, Particle hydrogels decrease cerebral atrophy and attenuate astrocyte and microglia/macrophage reactivity after stroke, Adv. Ther. 5 (2022) 1–15.
[24] Q. Feng, Q. Li, H. Wen, J. Chen, M. Liang, H. Huang, D. Lan, H. Dong, X. Cao, Injection and self-assembly of bioinspired stem cell-laden gelatin/hyaluronic acid hybrid microgels promote cartilage repair in vivo, Adv. Funct. Mater. 29 (2019) 1906690.
[25] T.P.T. Nguyen, F. Li, S. Shrestha, R.S. Tuan, H. Thissen, J.S. Forsythe, J.E. Frith, Cell-laden injectable microgels: current status and future prospects for cartilage regeneration, Biomaterials 279 (2021) 121214.
[26] Y. Zhu, Y. Sun, B. Rui, J. Lin, J. Shen, H. Xiao, X. Liu, Y. Chai, J. Xu, Y. Yang, A photoannealed granular hydrogel facilitating hyaline cartilage regeneration via improving chondrogenic phenotype, 14 (2022) 40674–40687.
[27] X. Ren, M. Zhao, B. Lash, M.M. Martino, Z. Julier, Growth factor engineering strategies for regenerative medicine applications, Front. Bioeng. Biotechnol. 7 (2020) 1–9.
[28] C. Iglesias-López, A. Agustí, M. Obach, A. Vallano, Regulatory framework for advanced therapy medicinal products in Europe and United States, Front. Pharmacol. 10 (2019) 1–14.
[29] M.M. Martino, P.S. Briquez, E. Güç, F. Tortelli, W.W. Kilarski, S. Metzger, J.J. Rice, G.A. Kuhn, R. Müller, M.A. Swartz, J.A. Hubbell, Growth factors engineered for super-affinity to the extracellular matrix enhance tissue healing, Science 343 (2014) 885–889.
[30] P.S. Briquez, H.M. Tsai, E.A. Watkins, J.A. Hubbell, Engineered bridge protein with dual affinity for bone morphogenetic protein-2 and collagen enhances bone regeneration for spinal fusion, Sci. Adv. 7 (2021).
[31] L.J. Pruett, C.H. Jenkins, N.S. Singh, K.J. Catallo, D.R. Griffin, Heparin microislands in microporous annealed particle scaffolds for accelerated diabetic wound healing, Adv. Funct. Mater 31 (2021) 2104337.
[32] E. Öztürk, Ø. Arlov, S. Aksel, L. Ling, D.M. Ornitz, G. Skjåk-Bræk, M. Zenobi-Wong, Sulfated hydrogel matrices direct mitogenicity and maintenance of chondrocyte phenotype through activation of FGF signaling, Adv. Funct. Mater. 26 (2016) 3649–3662.
[33] N. Banik, S. Bin Yang, T.B. Kang, J.H. Lim, J. Park, Heparin and its derivatives: challenges and advances in therapeutic biomolecules, Int. J. Mol. Sci. 22 (2021).
[34] S. Chasan, E. Hesse, P. Atallah, M. Gerstner, S. Diederichs, A. Schenker, K. Grobe, C. Werner, W. Richter, Sulfation of glycosaminoglycan hydrogels instructs cell fate and chondral versus endochondral lineage decision of skeletal stem cells in vivo, Adv. Funct. Mater. 32 (2021) 2109176.
[35] B. Wang, P.J. Díaz-Payno, D.C. Browe, F.E. Freeman, J. Nulty, R. Burdis, D.J. Kelly, Affinity-bound growth factor within sulfated interpenetrating network bioinks for bioprinting cartilaginous tissues, Acta Biomater. 128 (2021) 130–142.
[36] Q. Feng, S. Lin, K. Zhang, C. Dong, T. Wu, H. Huang, X. Yan, L. Zhang, G. Li, L. Bian, Sulfated hyaluronic acid hydrogels with retarded degradation and enhanced growth factor retention promote hMSC chondrogenesis and articular cartilage integrity with reduced hypertrophy, Acta Biomater. 53 (2017) 329–342.
[37] Ø. Arlov, D. Rütsche, M. Asadi Korayem, E. Öztürk, M. Zenobi-Wong, Engineered sulfated polysaccharides for biomedical applications, Adv. Funct. Mater. 31 (2021) 1–52.
[38] Y. Lei, Y. Wang, J. Shen, Z. Cai, Y. Zeng, P. Zhao, J. Liao, C. Lian, N. Hu, X. Luo, W. Cui, W. Huang, Stem cell-recruiting injectable microgels for repairing osteoarthritis, Adv. Funct. Mater 31 (2021) 2105084.
[39] J.M. Lee, B.S. Kim, H. Lee, G. Il Im, In vivo tracking of mesechymal stem cells using fluorescent nanoparticles in an osteochondral repair model, Mol. Ther. 20 (2012) 1434–1442.
[40] Y. Mishima, M. Lotz, Chemotaxis of human articular chondrocytes and mesenchymal stem cells, J. Orthop. Res. 26 (2008) 1407–1412.
[41] J. Fiedler, N. Etzel, R.E. Brenner, To go or not to go: Migration of human mesenchymal progenitor cells stimulated by isoforms of PDGF, J. Cell. Biochem. 93 (2004) 990–998.
[42] K. Endo, K. Horiuchi, H. Katano, N. Ozeki, Y. Sakamaki, H. Koga, I. Sekiya, Intra-articular injection of PDGF-BB explored in a novel in vitro model mobilizes mesenchymal stem cells from the synovium into synovial fluid in rats, Stem Cell Rev. Rep. 17 (2021) 1768–1779.
[43] M.L. Vainieri, A. Lolli, N. Kops, D. D'Atri, D. Eglin, A. Yayon, M. Alini, S. Grad, K. Sivasubramaniyan, G.J.V.M. van Osch, Evaluation of biomimetic hyaluronic-based hydrogels with enhanced endogenous cell recruitment and cartilage matrix formation, Acta Biomater. 101 (2020) 293–303.
[44] Y. Ozaki, M. Nishimura, K. Sekiya, F. Suehiro, M. Kanawa, H. Nikawa, T. Hamada, Y. Kato, Comprehensive analysis of chemotactic factors for bone marrow mesenchymal stem cells, Stem Cells Dev. 16 (2007) 119–129.
[45] P.H. Liebesny, S. Byun, H.H. Hung, J.R. Pancoast, K.A. Mroszczyk, W.T. Young, R.T. Lee, D.D. Frisbie, J.D. Kisiday, A.J. Grodzinsky, Growth factor-mediated migration of bone marrow progenitor cells for accelerated scaffold recruitment, Tissue Eng. Part A. 22 (2016) 917–927.
[46] M. Kesti, M. Müller, J. Becher, M. Schnabelrauch, M. D'Este, D. Eglin, M. Zenobi-Wong, A versatile bioink for three-dimensional printing of cellular scaffolds based on thermally and photo-triggered tandem gelation, Acta Biomater. 11 (2015) 162–172.
[47] M. Müller, P. Fisch, M. Molnar, S. Eggert, M. Binelli, K. Maniura-Weber, M. Zenobi-Wong, Development and thorough characterization of the processing steps of an ink for 3D printing for bone tissue engineering, Mater. Sci. Eng. C 108 (2020) 110510.
[48] M.Y. Kwon, S.L. Vega, W.M. Gramlich, M. Kim, R.L. Mauck, J.A. Burdick, Dose and timing of N-cadherin mimetic peptides regulate MSC chondrogenesis within hydrogels, Adv. Healthc. Mater. 7 (2018) 1–10.
[49] R. Li, S. Lin, M. Zhu, Y. Deng, X. Chen, K. Wei, J. Xu, G. Li, L. Bian, Synthetic presentation of noncanonical Wnt5a motif promotes mechanosensing-dependent differentiation of stem cells and regeneration, Sci. Adv. 5 (2019).
[50] J.Y. Tinevez, N. Perry, J. Schindelin, G.M. Hoopes, G.D. Reynolds, E. Laplantine, S.Y. Bednarek, S.L. Shorte, K.W. Eliceiri, TrackMate: An open and extensible platform for single-particle tracking, Methods 115 (2017) 80–90.
[51] D. Ershov, M. Phan, J.W. Pylvänäinen, S.U. Rigaud, L.Le Blanc, J.R.W. Conway, R.F. Laine, N.H. Roy, D. Bonazzi, G. Duménil, G. Jacquemet, J. Tinevez, Bringing TrackMate into the era of machine-learning and deep-learning, BioRxiv (2021) 1–4.
[52] K. Flégeau, A. Puiggali-jou, M. Zenobi-wong, Cartilage tissue engineering by extrusion bioprinting utilizing porous hyaluronic acid microgel bioinks Cartilage tissue engineering by extrusion bioprinting utilizing porous hyaluronic acid microgel bioinks, Biofabrication 14 (2022) 034105.
[53] A. Yasin, Y. Ren, J. Li, Y. Sheng, C. Cao, K. Zhang, Advances in Hyaluronic Acid for Biomedical Applications 10 (2022) 1–12.
[54] F. Yousefi, S. Kandel, N. Pleshko, Infrared spectroscopic quantification of methacrylation of hyaluronic acid: a scaffold for tissue engineering applications, Appl. Spectrosc. 72 (2018) 1455–1466.
[55] V.G. Muir, H.Q. Taimoor, S. Junwen, J. Groll, J.A. Burdick, Influence of microgel fabrication technique on granular hydrogel properties, ACS Biomater. Sci. Eng. 7 (2021) 4269–4281.
[56] T.H. Qazi, J. Wu, V.G. Muir, S. Weintraub, S.E. Gullbrand, D. Lee, D. Issadore, J.A. Burdick, Anisotropic rod-shaped particles influence injectable granular hydrogel properties and cell invasion, Adv. Mater. 34 (2022).
[57] V.G. Muir, T.H. Qazi, S. Weintraub, B.O. Torres Maldonado, P.E. Arratia, J.A. Burdick, Sticking together: injectable granular hydrogels with increased functionality via dynamic covalent inter-particle crosslinking, Small 2201115 (2022) 1–14.
[58] P.S. Lienemann, Q. Vallmajo-Martin, P. Papageorgiou, U. Blache, S. Metzger, A.S. Kiveliö, V. Milleret, A. Sala, S. Hoehnel, A. Roch, R. Reuten, M. Koch, O. Naveiras, F.E. Weber, W. Weber, M.P. Lutolf, M. Ehrbar, Smart hydrogels for the augmentation of bone regeneration by endogenous mesenchymal progenitor cell recruitment, Adv. Sci. 7 (2020) 1903395.

[59] P.H. Wu, A. Giri, S.X. Sun, D. Wirtz, Three-dimensional cell migration does not follow a random walk, Proc. Natl. Acad. Sci. U. S. A. 111 (2014) 3949–3954.
[60] F. Anjum, P.S. Lienemann, S. Metzger, J. Biernaskie, M.S. Kallos, M. Ehrbar, Enzyme responsive GAG-based natural-synthetic hybrid hydrogel for tunable growth factor delivery and stem cell differentiation, Biomaterials 87 (2016) 104–117.
[61] S.J. Heo, K.H. Song, S. Thakur, L.M. Miller, X. Cao, A.P. Peredo, B.N. Seiber, F. Qu, T.P. Driscoll, V.B. Shenoy, M. Lakadamyali, J.A. Burdick, R.L. Mauck, Nuclear softening expedites interstitial cell migration in fibrous networks and dense connective tissues, Sci. Adv. 6 (2020) 1–13.
[62] M.T. Wei, S. Elbaum-Garfinkle, A.S. Holehouse, C.C.H. Chen, M. Feric, C.B. Arnold, R.D. Priestley, R.V. Pappu, C.P. Brangwynne, Phase behaviour of disordered proteins underlying low density and high permeability of liquid organelles, Nat. Chem. 9 (2017) 1118–1125.
[63] H. Chen, E.E. Konofagou, The size of blood-brain barrier opening induced by focused ultrasound is dictated by the acoustic pressure, J. Cereb. Blood Flow Metab. 34 (2014) 1197–1204.
[64] F. Li, C. Levinson, V.X. Truong, L.A. Laurent-Applegate, K. Maniura-Weber, H. Thissen, J.S. Forsythe, M. Zenobi-Wong, J.E. Frith, Microencapsulation improves chondrogenesis: In vitro and cartilaginous matrix stability in vivo compared to bulk encapsulation, Biomater. Sci. 8 (2020) 1711–1725.
[65] J. Lee, J.J. Yoo, A. Atala, S.J. Lee, The effect of controlled release of PDGF-BB from heparinconjugated electrospun PCL/gelatin scaffolds on cellular bioactivity and infiltration, 33 (2013) 6709–6720.
[66] N. Broguiere, E. Cavalli, G.M. Salzmann, L.A. Applegate, M. Zenobi-Wong, Factor XIII cross-linked hyaluronan hydrogels for cartilage tissue engineering, ACS Biomater. Sci. Eng. 2 (2016) 2176–2184.